Adsorption of REEs to kaolinite via ion exchange and surface complexation as a function of water chemistry

Elmira Ramazanova[1], Neha Sharma[1], Elaine D. Flynn[2], Olwen Stagg[2], Jeffrey G. Catalano[2], Daniel E. Giammar[1,*]

[1]Department of Energy, Environmental and Chemical Engineering, Washington University in St. Louis, St. Louis, Missouri 63130, United States

[2]Department of Earth, Environmental, and Planetary Sciences, Washington University in St. Louis, St. Louis, Missouri 63130, United States

*Corresponding Author:

Address: Department of Energy, Environmental and Chemical Engineering, Washington University in St. Louis, St. Louis, MO 63130, USA

Phone: 314-935-6849

Email: giammar@wustl.edu

Revised manuscript submitted to *ACS Earth and Space Chemistry*

May 2025

Abstract

Rare earth elements (REEs) are critical components of modern technology behind renewable energy, transportation, and electronics but have a limited current supply. A substantial portion of global REE production relies on ion adsorption deposits. A high abundance of kaolinite in REE enrichment zones within these deposits suggests that kaolinite controls the subsurface migration of REEs. This study aimed to improve the current understanding of REE binding to kaolinite under varying water chemistry conditions. We conducted batch experiments with kaolinite (KGa-2) and three REEs (Nd, Dy, and Yb) at varying pH, electrolyte concentration, dissolved inorganic carbon (DIC), low molecular weight organic acids (citric and oxalic acids), and total REE concentration conditions. Increasing electrolyte concentration inhibits REE adsorption at pH < 7, suggesting that ion exchange contributes to adsorption at these pH values. DIC affects adsorption above pH 7-8 by forming a strong aqueous complex with heavy REEs. Citric acid decreases REE adsorption via aqueous complexation of REEs at pH > 5 but does not affect adsorption at pH < 5. The surface complexation model captures the main adsorption trends with two mechanisms: ion exchange on basal planes at pH < ~6 and inner-sphere surface complexation to edge sites at pH > ~6. Equilibrium constants for surface complexation increase in the order of Yb > Dy > Nd, indicating a higher strength of adsorption for heavy REEs. This study demonstrates how water chemistry conditions can control the adsorption mechanisms that may determine the mobility of REEs in subsurface environments rich in kaolinite.

Keywords: rare earth elements, kaolinite, adsorption, clay, surface complexation modeling, dissolved inorganic carbon.

40 Table of Contents (TOC) graphic

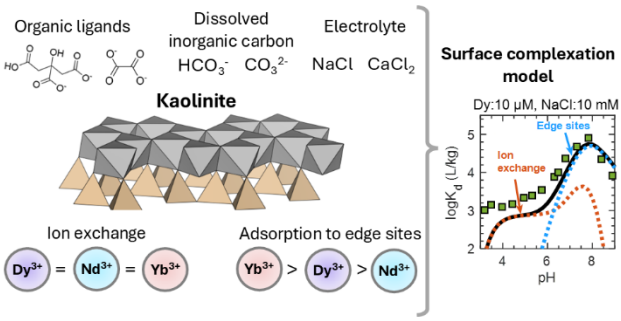

41

1. Introduction

Unique magnetic, optical, and electrical properties of rare earth elements (REEs), also known as lanthanides, make them key components in many critical applications, such as lasers, optical sensors, magnets, wind turbines, and additives in alloys.[1] As a result, different industries involving sustainable energy generation, medicine, defense, and the production of electronic technology depend on a continuous supply of REEs.[2] Demand for these elements has increased in recent years and is projected to grow.[3,4] Exports of REEs are limited to only a few countries, mainly China, resulting in price volatility and uncertainty in the future of the steady availability of critical elements.[5] Around 35% of all Chinese REE production comes from ion adsorption deposits (IADs).[6] The occurrence of IADs is not limited to China; they are also present in Japan, Madagascar, the United States, Australia, Brazil, and countries in Southeast Asia.[7,8] IADs are known for their easy extractability and lower costs of exploitation, unlike other more abundant deposits such as alkaline and carbonate rocks.[9,10] They are also selective to heavy REEs (Gd to Lu), providing ~80% of all heavy REEs globally.[11] As numerous countries search for alternative REE sources,[3] it is important to develop a fundamental understanding of geochemical processes governing the retention of REEs in IADs.

IADs are formed by the weathering of granitic bedrock. Although granite is the most commonly reported rock type found in IADs,[12–15] some studies report the presence of other igneous rocks (syenite,[12,14] pegmatite,[14] and monzonite[12]) and volcanic rocks.[10,12,14] Granite bedrock hosts REE-containing accessory minerals such as silicates, phosphates, fluorocarbonates, and fluorides.[10,12] Weathering promotes dissolution of these accessory minerals, releasing REEs to groundwater.[10,15] The released REE species are retained by adsorption to weathering products, primarily clays.[12]

Kaolinite, along with illite and halloysite, is one of the most abundant clay minerals in the REE-enriched zone of IADs.[16–18] Kaolinite, a 1:1 clay, consists of ~7 Å wide flat sheets comprised of Si tetrahedra and Al octahedra layers.[19] Kaolinite has different surfaces: basal planes and edge sites, which consist of amphoteric surface hydroxyl groups associated with Si or Al.[19] The high kaolinite content in IADs suggests that kaolinite plays an important role in the retention of REEs. Therefore, understanding surface binding in the kaolinite-REE system will help elucidate REE enrichment mechanisms in IADs.

REE adsorption on kaolinite has been explored at macroscopic and molecular levels. Batch studies have explored the adsorption edges of all REEs in the lanthanide group at different ionic strengths to determine if the dominant complex is outer- or inner-sphere. These batch studies[16,20,21] found that the background electrolyte concentration affects REE adsorption at lower pH (around 3-6), suggesting adsorption via outer-sphere complexation. Time-resolved laser fluorescence spectroscopy (TRLFS) studies mostly focused on Eu^{3+} and indicated that an outer-sphere complex dominates adsorption at pH < 4-5 and low ionic strength.[22,23] As pH increases, batch studies report an increase in adsorption.[16,21,24] TRLFS studies involving Eu^{3+} have reported the formation of inner-sphere complexes as pH increases,[22,23] although extended X-ray absorption fine structure (EXAFS) studies on Nd^{3+} and Y^{3+} indicate that outer-sphere complexes might be present at circumneutral or high pH.[14]

Water chemistry conditions relevant to weathering environments might affect REE binding to kaolinite. The weathering environment's pH is slightly acidic (4-5) closer to the surface and increases to pH 6-7 deeper in the enrichment zone.[15] Dissolved inorganic carbon (DIC) is present in IADs from the uptake of CO_2.[12] Some studies suggest the formation of ternary surface complexes of REEs with DIC on kaolinite.[23,25] Inorganic ions such as Cl^-, NO_3^-, and SO_4^{2-} are

present in weathering environments but they are unlikely to affect REE adsorption to kaolinite due to their negative charge and weak aqueous complexation with REEs.[26]

Dissolved organic matter is an umbrella term for a wide variety of dissolved organic compounds occurring in natural environments and is ubiquitous in weathering zones such as ion adsorption deposits.[27,28] These compounds can facilitate the release of REEs from minerals by forming aqueous complexes[11] or can retain REEs at the mineral surface by forming ternary surface complexes.[27] This dual effect of organic matter on REE adsorption was observed in studies involving humic acid; humic acid promotes REE adsorption (possibly through ternary complexes) at pH < 4, but decreases REE adsorption to kaolinite at pH > 4.[29,30] While the effect of humic acid on REE adsorption is known, the role of low molecular weight organic acids (LMWOAs) in REE adsorption had been considered in previous literature. LMWOAs are present in the top layers of weathering environments due to the exudation from roots and the degradation of organic matter.[31] The presence of vegetation over ion adsorption deposits[32] suggests that LMWOAs are present in the subsurface of the deposits and can affect REE adsorption to kaolinite. Among the most common LMWOAs are oxalic and citric acids.

A surface complexation model (SCM) describes equilibrium adsorption by considering chemical binding and electrostatic interactions between the surface of the mineral and surrounding aqueous ions. It provides a set of equilibrium constants for adsorption reactions, which can then be used to predict REE concentrations at a given water chemistry. A SCM's key strength is its applicability over a wide range of water chemistry conditions.[33] Therefore, the usefulness of SCM is proportional to the number of datapoints and experimental conditions upon which the model is built. SCMs can be used in reactive transport models to advance the understanding of the fate and transport of REE. Such models can also be helpful for understanding the formation of ion

adsorption deposits and developing possible recovery strategies by providing insights into the adsorption mechanism.

Although REE adsorption to clay minerals has been investigated in previous work,[21,24,25,33–35] the studies explored limited ranges of water chemistry conditions and metals. For example, many studies focused primarily on Eu^{3+} and did not explore the adsorption trends across the lanthanide series. Another overlooked water chemistry parameter is DIC. Previous studies of the REE-kaolinite system did not describe the effect of CO_2 on REE adsorption. The effect of LMWOAs has not been covered by REE-clay adsorption studies. Some studies have developed SCM for the REE-kaolinite system.[24,33] However, these SCMs were developed based on a limited dataset, restricting their predictive ability.[24,33]

The main objectives of this study were to (1) investigate how varying water chemistry (pH, background electrolyte conditions, total REE concentration, the presence of LMWOAs, and DIC) affects the extent of adsorption of light (Nd) and heavy (Dy and Yb) REEs to kaolinite, and (2) to interpret the surface speciation and binding mechanisms of REEs to kaolinite using surface complexation modeling and EXAFS. We aim to develop a robust model, which can be applied to diverse water chemistry conditions. Testing new water chemistry variables relevant to subsurface conditions in ion adsorption deposits will expand the current knowledge of adsorption in the REE-kaolinite system. Incorporating these water chemistry variables into a robust SCM will enhance our predictive ability to estimate REE behavior in the environment.

2. Materials and Methods

Reagents

Chemicals from Sigma-Aldrich used in batch experiments were $Nd(NO_3)_3 \cdot 6H_2O$ (99.9%, trace metal basis), $Yb(NO_3)_3 \cdot 8H_2O$ (99.9%, trace metal basis), $Dy(NO_3)_3 \cdot 5H_2O$ (99.9%, trace metal basis), sodium chloride, and sodium hydroxide (>98%, reagent grade). Citric acid (certified ACS grade), oxalic acid dihydrate (certified ACS grade), and nitric acid (67.7-70%, trace metal grade) were obtained from Fisher Scientific. Calibration standards for inductively coupled plasma mass spectroscopy (ICP-MS) were prepared from a standard obtained from Inorganic Ventures (3 % v/v HNO_3).

Kaolinite preparation and characterization

One batch of kaolinite clay powder (KGa-2) from the Source Clays Repository was used to prepare all kaolinite suspensions. KGa-2 kaolinite was chosen for its widespread use in adsorption studies, allowing comparison with other studies. Kaolinite was cleaned and size-fractionated using a published procedure.[36] The Brunauer−Emmett−Teller (BET) specific surface area is 21.5 m^2/g (N_2 adsorption, Quantachrome Nova 2000e). The effective cation exchange capacity (CEC) was determined by an additional experiment at pH 4 with no added electrolyte salt (more details in the section describing the effect of the total REE concentration). The negative charge observed in natural kaolinites is usually attributed to the isomorphic substitution of Si^{4+} by Al^{3+} in the tetrahedral sheet of kaolinite[37,38] but can also be due to the presence of smectite layers.[39,40] The hexagonal kaolinite plates have a size < 2 μm (Thermofisher Quattro S ESEM) (Figure S1).

Titration

Potentiometric titrations were performed to determine acid-base properties of surface sites of kaolinite in a solution containing 0.01 M NaCl and 5 g/L kaolinite under CO_2-free conditions (Coy Laboratory Products, filled with nitrogen gas) and at room temperature (22°C). The gas inside the glovebox was pumped through a 10 M KOH scrubber solution to ensure the absence of CO_2. Before starting each of the CO_2-free experiments, we confirmed that the pH value of the 0.01 M NaOH solution was 12. If CO_2 had infiltrated the glovebox from the air, the pH value of the 0.01 M NaOH would have been around 9.1. The starting pH was adjusted with 0.05 M HCl to the value of 3 and was raised to 9 by adding 5-50 μL of 0.03 M NaOH. Blank titrations were done under the same conditions as above, but without kaolinite.

Adsorption experiments

Adsorption edge experiments were done in 15-mL batch reactors at room temperature (22°C) with each REE separately (Nd or Dy or Yb) unless stated otherwise. Different sets of experiments were performed to encompass different water chemistry conditions. Background electrolyte conditions studied were 1 mM NaCl, 10 mM NaCl, and 10 mM $CaCl_2$. The addition of electrolyte is required to control the ionic strength at a fixed value. Our findings are relevant to groundwater with ionic strength ranging from 1 mM to 20 mM.

Adsorption edge experiments were done over the pH range of 3-9. Total REE concentrations were 1 and 10 μM. We observe almost no kaolinite dissolution based on measured Al concentrations (<0.1% kaolinite dissolved). Adsorption edge experiments with LMWOAs (citric and oxalic acids) were conducted in the presence of 100 μM organic ligand, 10 mM NaCl, and 10 μM of REE. The selected concentration of LMWOAs (100 μM) is within the range of the naturally occurring concentrations, from a few nM up to 1 mM in soils.[41] Two competitive adsorption experiments

were done by mixing all REEs (referred to as mixed batch experiments) at 1 μM and 10 μM concentrations of each REE (3 μM and 30 μM total REE concentrations, respectively) at 10 mM NaCl. In addition to adsorption edges, isotherm experiments were conducted at pH 6 and 10 mM NaCl in duplicate with total REE concentrations up to 100 μM. The effect of varying NaCl (1 - 100 mM) and $CaCl_2$ concentrations (1 - 7 mM) on REE adsorption was examined at pH 4. Kaolinite loading was 0.2 g/L in all experiments.

We used ultrapure water (18.2 MΩ·cm) that had been equilibrated with atmospheric CO_2 in all adsorption experiments (except for the CO_2-free adsorption edge experiment). Ultrapure water was purged with air before the start of the experiment at a pH that had been pre-adjusted to the desired value with $NaHCO_3$ to accelerate the process of equilibrating with atmospheric CO_2. The CO_2-free adsorption edge experiment was done in the glovebox (Coy Laboratory Products) in a nitrogen gas environment with 10 mM NaCl and 10 μM REE.

The first step of the experiments was mixing the stock solutions (1 M NaCl, 100-500 μM REE, 10 mM LMWOAs, and 10 g/L kaolinite) to achieve the desired concentrations of REE, kaolinite, electrolyte concentration, and, if necessary, LMWOAs. The stock suspension of kaolinite was vigorously mixed to ensure that kaolinite particles were distributed homogeneously during the addition of the mineral to the reactor. The suspension's pH was adjusted before adding REEs and re-adjusted immediately after the addition using small volumes (<5 μL) of HCl and NaOH. Samples were gently mixed on a rotator for 8-10 hours before further re-adjustment of pH values. After 24 h of equilibration, the pH was measured, and the solution was filtered through a 0.2 μm polyethersulfone (PES) syringe filter. The supernatant was measured by ICP-MS (PerkinElmer NexION 2000) after dilution and acidification to 1% HNO_3.

Adsorption calculations

Adsorption was quantified using both the logarithm of the distribution coefficient ($logK_d$, unit: $log_{10}(L\ kg^{-1})$) (Eq. 1) and percent adsorbed (Eq. 2). In isotherm experiments, adsorption was quantified with the adsorption density (μmol/g) (Eq. 3). C_{total} (μM) is the total concentration of REE in the reactor. A kaolinite-free control was prepared in every experiment to measure C_{total}. $C_{supernatant}$ (μM) is the concentration measured by ICP-MS after 24 h of equilibration. C_{ads} (μM) is the adsorbed concentration (Eq. 4). $C_{kaolinite}$ (kg/L) is the kaolinite loading (0.2 g/L in all experiments). $LogK_d$ values reveal adsorption trends more clearly than the percent adsorbed when adsorption is high. When adsorption is low, however, adsorption trends are more apparent when plotted on the percent adsorbed scale. All figures from the main text that are plotted using $logK_d$ are included with the percent adsorbed scale in the supporting information. The range of the reported $logK_d$ values is 2 to 8. The upper limit depends on the detection limits of ICP-MS, which were calculated during every measurement and varied from 10 to 50 ng/L for all REEs. The lower limit denotes a $logK_d$ value below which adsorption is negligible (< 2%) and adsorption uncertainties become too high (±1 $logK_d$ units and larger). Uncertainties of the measured concentrations from ICP-MS (δ) were calculated based on weighted calibration equations (details are in the supporting information).

$$\log K_d = \log_{10}\left(\frac{C_{ads}}{C_{supernatant} \times C_{kaolinite}}\right) \quad \text{(Eq. 1)}$$

$$\%\text{adsorbed} = \frac{C_{ads}}{C_{total}} \times 100 \quad \text{(Eq. 2)}$$

$$\text{Adsorption density} = \frac{C_{ads}}{C_{kaolinite}} \quad \text{(Eq. 3)}$$

$$C_{ads} = C_{total} - C_{supernatant} \quad \text{(Eq. 4)}$$

X-ray absorption spectroscopy measurements

The L_3-edge X-ray absorption spectra of Yb adsorbed to kaolinite were measured at the Stanford Synchrotron Radiation Lightsource (SSRL) at beamlines 4-1, 4-3, and 11-2. Selected batch adsorption experiments covering varying water chemistry conditions (1-10 mM NaCl, pH 3.5-7, and 0-100 μM citric acid) were repeated in a scaled-up 500-mL reactor with 0.2 g/L kaolinite loading and 10 μM total REE concentration to obtain 1000-7700 μg REE/g kaolinite surface coverage. Samples were prepared following the same procedures as for the adsorption studies, after which they were centrifuged, and the supernatant was decanted. The remaining wet pastes of reacted kaolinite were then sealed in Delrin sample holders using Kapton tape. Cryogenically-cooled Si double-crystal monochromators were used for energy scanning, with the (111) orientation employed at beamline 4-3 and the (220) orientation at beamlines 4-1 and 11-2. All data were collected in fluorescence yield using a 7-element silicon drift detector (4-3), a 32-element energy-dispersive Ge detector (4-1), or a 100-pixel segmented Ge array detector (11-2). Four to ten scans were collected for each sample and then averaged to increase the signal-to-noise ratio. Data were averaged in the SixPack interface[42] to IFEFFIT,[43] followed by background removal and FEFF-based structural model fitting of the extended X-ray absorption fine structure (EXAFS) region in Larch.[44] Backscattering phase and amplitude functions for analysis were calculated in FEFF 8L[45] using the crystal structure of $Yb_5Al_3O_{12}$.[46] Spectra were also collected for Nd adsorbed to kaolinite but contained substantial artifacts near k = 7.7 $Å^{-1}$ (at the Pr L_2-edge) and 9.4 $Å^{-1}$ (at the Ce L_1-edge) in the EXAFS region. Kaolinite KGa-2 contains 56±8 mg/kg Ce and 6.0±0.9 mg/kg Pr.[47] Similarly, the Fe content of KGa-2 (1.15 wt.% as Fe_2O_3)[48] produced a substantial X-ray fluorescence background signal that prevented measurement of spectra of Dy adsorbed to kaolinite KGa-2. The Yb spectra did not suffer from spectral artifacts because of the substantially lower content of heavy REEs in KGa-2[48] and the separation of the Yb L_3-edge from the Fe K-edge.

Surface complexation modeling

We developed an SCM in Visual MINTEQ 3.1 to aid in the interpretation of the results.[49] Visual MINTEQ 3.1 is a common software used for calculating aqueous and surface speciation.[50] The thermodynamic database for stability constants and solubility products of REEs is summarized in Table S1. Solubility and speciation diagrams of REEs are provided in the supporting information (Figures S2 and S3, respectively). The Davies equation was used to calculate activity coefficients. Model parameters were found by minimizing the residual sum of squares (RSS) between the experimentally observed and model-calculated logarithms of total dissolved concentration. Intrinsic equilibrium constants (logK values) were optimized to the nearest 0.1 units. A detailed overview of the fitting procedure is in the supplementary information.

3. Results and Discussion

Effects of pH and DIC

REEs adsorb to kaolinite at pH < 5 to a limited extent and independently of pH ($logK_d$ of ~3 or 10-20% adsorbed) (Figure 1). All plots are re-plotted as %adsorbed in the supporting information (Figures S4-S8). Adsorption of REEs increases with increasing pH, with a major rise occurring between pH values of 6 to 7 (around 0.5-1.2 $logK_d$ units or 30-50% adsorbed). Overall, the effect of pH on REE retention to kaolinite agrees with other studies involving REEs and other cations.[51]

Without DIC, $logK_d$ values increased with pH, reaching 5.8 (Nd), 6.5 (Dy), and 6.7 (Yb) at pH values of 8.2-8.8. In the presence of atmospheric CO_2, $logK_d$ values decrease at pH > 8. Complexation with carbonate ligands might cause the observed decrease in retention. DIC affects the aqueous chemistry of REEs by forming $REECO_3^+$ or $REE(CO_3)_2^-$ complexes (Figure S2). In the presence of DIC, REEs are present as REE^{3+} at low pH values and as $REECO_3^+$ above pH~7. A strong $REE(CO_3)_2^-$ aqueous complex is the main form of REE above pH 8 for Yb, 8.1 for Dy, and 8.3 for Nd. Stability constants of both $REECO_3^+$ and $REE(CO_3)_2^-$ follow the order of Yb > Dy > Nd (Table S1), indicating stronger complexation with heavier REEs.

Some experiments involved water chemistry conditions at which solubility calculations predict the precipitation of REEs if no adsorption were to occur (Figure S3). In CO_2-free experiments with 10 μM total REE (Figure 1), solubility calculations predict precipitation of $Nd(OH)_3(s)$ above pH 7.9, $Dy(OH)_3(s)$ above pH 7.2, and $Yb(OH)_3(s)$ above pH 7. When atmospheric CO_2 is present (Figure 1), $REE(OH)_3(s)$ is predicted to remain a solubility-controlling solid for Dy (pH > 7.4) and Yb (pH > 7.1), but Nd is predicted to precipitate as $Nd_2(CO_3)_3(s)$ (pH > 7.2). If data points are at conditions below solubility limits (solid-colored markers), then precipitation is ruled out as a retention

mechanism and the observed $\log K_d$ value can be unequivocally attributed to adsorption. However, if the data points are at conditions above solubility limits (open white markers), then precipitation, adsorption, or both could have occurred. When referring to data points at which REE precipitation is calculated in the absence of adsorption, we use "retention" instead of "adsorption" and indicate these data points with open white markers. SCM can help distinguish if precipitation contributes to the observed retention at pH values where REEs could precipitate in case adsorption did not lower the dissolved REE concentration below solubility limits. To avoid the effect of precipitation on the development of the SCM, all data points for which precipitation could occur (open white markers) were not included in model optimization.

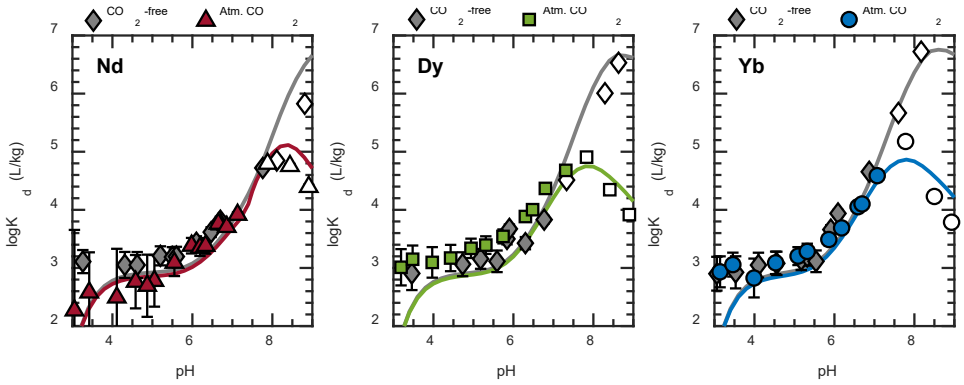

Figure 1. The effect of pH and DIC in equilibrium with atmospheric CO_2 on the retention of REEs (10 μM) to kaolinite (0.2 g/L) in the presence of 10 mM NaCl. Markers represent experimental data; open white markers show data points at which solubility calculations indicate the possibility of REE precipitation. Solid lines represent the output from the SCM.

Effect of electrolyte cations

Increasing electrolyte concentration decreases REE adsorption at pH 4 (Figure 2). The dependence of adsorption on the electrolyte concentration indicates that ion exchange reactions dominate adsorption at pH 4. Divalent cations (Ca^{2+}) suppress adsorption to a greater extent than monovalent cations (Na^{+}) at an equivalent ionic strength, as can be seen for Nd adsorption (Figure 2). REEs are present in the form of REE^{3+} under a pH value of ~7 regardless of the presence of DIC (Figure S2), suggesting that REEs can adsorb via an ion exchange mechanism up to pH ~7. Divalent

cations could occupy more sites on basal planes, saturating more available sites than monovalent cations at the same concentration. Divalent cations could also adsorb more strongly than monovalent ions.

Ion exchange reactions are known to be important in the adsorption of cations to basal planes of clay minerals, including kaolinite.[24,52] However, kaolinite is a 1:1 clay and in its purest stoichiometric form would not have any charge compensation for isomorphic substitutions that result in permanently charged basal planes.[19] It has been previously suggested that the isomorphic substitution of Al by Si in an octahedral sheet or the mixing of smectite layers in natural kaolinite might be responsible for the observed cation exchange capacity in natural kaolinites (CEC).[38,39]

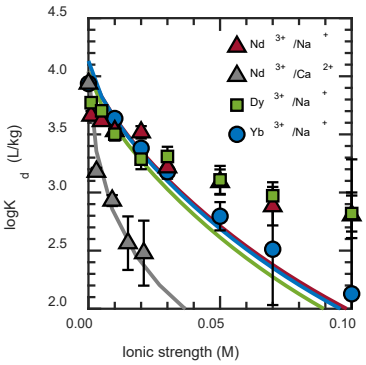

Figure 2. The effect of electrolyte type (NaCl and $CaCl_2$) and concentration on adsorption of REEs (1 µM) to kaolinite at pH 4. The solutions in all experiments were in equilibrium with atmospheric CO_2. Markers represent experimental data; solid lines represent the output from the SCM.

The presence of different electrolyte types and concentrations (10 mM NaCl, 1 mM NaCl, and 10 mM $CaCl_2$) affects REE adsorption to kaolinite at pH values above 4 (Figure 3). At pH < ~6.5, the electrolyte affects adsorption similarly to at pH 4, i.e., increasing the concentration and the charge of the electrolyte decreases REE adsorption. At pH 7, adsorption edges corresponding to 10 µM total Nd concentration and different electrolyte conditions become more similar, indicating that the effect of electrolyte type and concentration fades at higher pH (Figure 3, right panel). In 1 µM

Nd experiments, adsorption edges corresponding to 10 mM NaCl and 10 mM $CaCl_2$ become more similar at pH 7 but do not converge with the adsorption edge corresponding to 1 mM NaCl (Figure 3, left panel). The independence of adsorption trends from the electrolyte's type and concentration indirectly suggests that REEs form inner-sphere complexes on kaolinite's surface.[52,53] Inner-sphere complexation involves chemical binding to a hydroxyl group on a mineral's surface (edge sites), that is not mediated by water molecules and is less dependent on the electrolyte.[51–53] The results suggest that inner-sphere complexation becomes more important as pH increases. The poor convergence of the adsorption edge of 1 µM Nd in the presence of 1 mM NaCl with the adsorption edges with 10 mM NaCl and 10 mM $CaCl_2$ suggests that adsorption depends on the electrolyte type and concentration and that inner-sphere complexation is unlikely to happen at these water chemistry conditions.

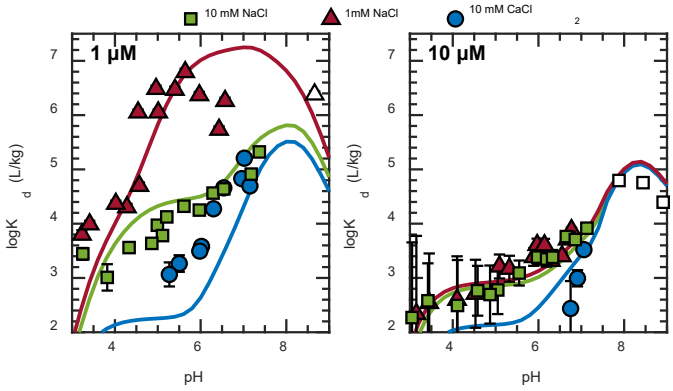

Figure 3. The effect of electrolyte type and concentration on Nd retention to kaolinite (0.2 g/L). Total Nd concentration was 1 µM and 10 µM. The solutions in all experiments were in equilibrium with atmospheric CO_2. Markers represent experimental data; open white markers show data points at which solubility calculations indicate the possibility of REE precipitation. Solid lines represent the output from the surface complexation model.

Effect of the total REE concentration

The total REE concentration affects REE adsorption when viewed on $logK_d$, %adsorbed, and adsorption density scales (Figure S9). Experiments with 10 µM total REE concentration do have higher adsorption densities than in 1 µM REE experiments for comparable pH (Figure S9);

however, adsorption affinity as represented by $\log K_d$ and %adsorbed is lower for 10 μM total REE loadings than 1 μM REE loadings (Figures S9, 3, and S6). The observed decrease in $\log K_d$ values at higher REE concentrations at low pH values suggests that the availability of adsorption sites is a limiting factor for adsorption. At low pH values (< 5), where ion exchange governs REE binding to kaolinite, a measure of maximum adsorption is cation exchange capacity (CEC).

The CEC of kaolinite KGa-2 was previously reported to be 37 meq/kg using the ammonia acetate method at pH 7.[54] The ammonia acetate method is known to overestimate CEC because it is done at a high pH value, at which pH-dependent edge sites can possibly affect the measurement of CEC.[55] To provide a better estimate of the effective CEC for our processed kaolinite and minimize the contribution from pH-dependent edge sites, we conducted an experiment with 5 μM Yb and no added NaCl to reduce the suppressing effect of an electrolyte at pH 4. We chose to estimate CEC at pH 4 because adsorption at this pH is governed mainly by ion exchange, as demonstrated in Figure 2, which shows that adsorption is a function of the electrolyte concentration at pH 4. The experiment showed the adsorbed Yb concentration of 1.5±0.3 μM (or 4.5±0.9 μeq/L), indicating a CEC of 22.5±4.5 meq/kg (1.5 μmol/L * 10^{-3} mmol/μmol * 3 eq/mol * 1/0.2 L/g * 10^3 g/kg). Although the CEC estimation method we used is unconventional, the determined CEC (22.5 meq/kg) falls within the reported range of CECs for KGa-2 kaolinite measured with different methods (9-37 meq/kg).[37,54,56] We assumed that the adsorbed Yb concentration from this experiment is indicative of the CEC. This result agrees with the observation from Figure 3 because the CEC of 22.5 meq/kg (or 1.5 μM REE) would limit the adsorption of 10 μM REE but not 1 μM REE. Although CEC does not restrict adsorption when the REE concentration is 1 μM, adsorption is lower than 100% (40-60% or $\log K_d$ of 2-3) at pH < 5 and 10 mM NaCl because $REEs^{3+}$ compete with Na^+ and H^+ ions for ion exchange sites.

We estimated the site density of edge sites by conducting the isotherm experiment, in which we increased the total REE concentration up to 100 μM at pH 6 and 10 mM NaCl (Figure 4). The maximum adsorption capacity is twice as high for Dy and Yb (96-113 μmol/g or 19-23 μM REE) as it is for Nd (59 μmol/g or 12 μM REE). We assume that the observed maximum adsorption capacity corresponds to the site density of edge sites. Ion exchange contributes to adsorption at pH 6 too, but its effect is assumed to be minimal because the maximum adsorbed REE concentration due to ion exchange is limited by CEC (22 meq/kg or 1.5 μM REE) and will account only for < 7% of the observed maximum adsorption capacity (23 μM). Assuming mono-nuclear and mono-dentate adsorption, the maximum adsorption capacity (23 μM) corresponds to an edge site density of 3.2 nm^{-2} of BET surface area (0.2 g/L kaolinite, 21.5 m^2/g BET surface area). The obtained site density agrees with other modeling studies reporting site densities in the range of 2.3-3.5 nm^{-2} based on BET surface area.[57–59] Although many SCM studies report site density of kaolinite per unit BET surface area, it is important to note that the BET surface area does not represent the surface area of edge sites. Edge sites can constitute 8 to 40% of kaolinite's BET surface area.[60–62] If we assume that edge sites constitute 40% of BET surface area, the obtained site density (3.2 nm^{-2} BET surface area) can be converted to 8.1 nm^{-2} edge surface area, a value in good agreement with crystallographic calculations by White and Zelazny (8.2 nm^{-2} edge surface area).[63] In this study, we assumed a site density of 3.3 nm^{-2} BET surface area, which is equivalent to the site density of 8.2 nm^{-2} edge surface area (assuming that edges contribute to 40% of BET surface area).

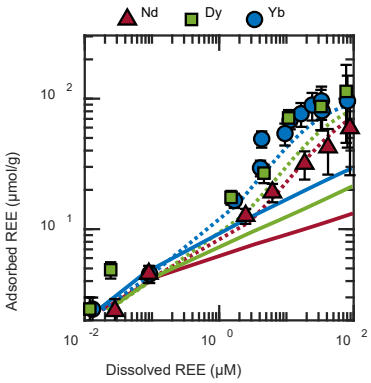

Figure 4. The effect of total REE concentration (0.1-100 µM) on REE adsorption to kaolinite (0.2 g/L) at pH 6±0.2 in the presence of 10 mM NaCl. Markers represent experimental data. Solid lines represent the output from the SCM; dotted lines represent the output from NEM. The solutions in all experiments were in equilibrium with atmospheric CO_2.

Competitive adsorption experiments

In the competitive adsorption experiments, 0.2 g/L kaolinite and all three REEs were mixed (mixed batch) as opposed to the rest of the experiments in which only one REE (separate batch) was present in the kaolinite suspension (Figure S10). Figure S11 compares data from mixed and separate batches for each REE and total concentration. The retention of each REE in the mixed batch experiment is lower or equivalent to the retention of the same REE in the separate batch experiment because REEs compete for the limited sites. A decrease in retention due to DIC in equilibrium with atmospheric CO_2 levels above pH 8 is in agreement with Figure 1.

The extent of retention in mixed batches is similar for all REEs, indicating little to no preference for any REE. This result contrasts the trend observed in separate batches (Figure 1), where retention increases as REEs become heavier, and in isotherm experiments, which indicated that Nd's maximum adsorption capacity is about half that of Dy and Yb. Differences in REE retention might vary slightly within the calculated uncertainties. Alternatively, there remains a possibility that other processes affect REE retention in a mixed batch.

Effect of low molecular weight organic acids

Citric and oxalic acids are common LMWOAs in weathering environments[41] and can affect the subsurface mobility of REEs. Citric acid does not affect adsorption at lower pH values (< 5), where ion exchange is the primary adsorption mechanism, but it substantially decreases adsorption at higher pH values (> 5) (Figure 5). Aqueous speciation diagrams (Figure S2) show that citric acid forms a neutrally charged REECit aqueous complex, the dominant form of REEs between pH values of 3 and 9. The formation of REECit(aq) complexes is expected to decrease adsorption by limiting REE^{3+} concentrations available for surface complexation in the studied pH range (3-9). At pH > 5, the decreased adsorption in the system containing citric acid can be explained by the presence of REECit(aq). At pH < 5, however, adsorption is unaffected by citric acid despite lower REE^{3+} concentrations predicted by thermodynamic calculations. The formation of ternary surface complexes (REE-citric acid-kaolinite) might explain the observed adsorption at pH < 5. Oxalic acid has little to no effect on REE adsorption (Figure S12). The effect of oxalic acid was investigated in the supporting information.

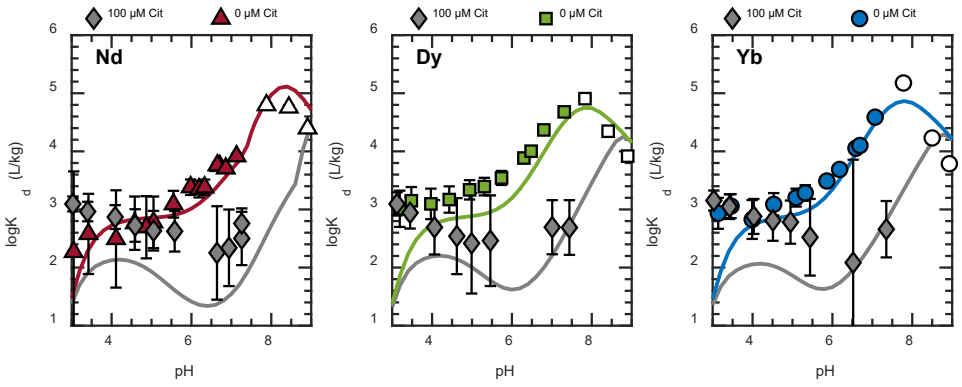

Figure 5. The effect of citric acid (100 µM) on the retention of REEs (10 µM) to kaolinite in the presence of 10 mM NaCl. The solutions in all experiments were in equilibrium with atmospheric CO_2. Markers represent experimental data; open white markers show data points at which solubility calculations indicate the possibility of REE precipitation. Solid lines represent the output from the SCM. The system with binary reactions, where citric acid and REEs adsorb to kaolinite separately, was assumed to model the experiment containing 100 µM citric acid (grey solid lines).

Extended X-ray absorption fine structure spectroscopy

The EXAFS spectra of Yb adsorbed to kaolinite were collected for samples in (a) 10 mM NaCl solution at pH 3.5, 6.0, and 7.0, (b) 1 mM NaCl at pH 4, and (c) 10 mM NaCl containing 100 μM citric acid at pH 3.5 and 7 (Figure 6). The spectra of citrate-free samples at pH 3.5 and 4 display similar features (Figure 6), with strong oscillations displayed throughout the entire data range. The Fourier transform feature associated with the first coordination shell was inadequately reproduced by a single O neighbor, suggesting asymmetric disorder. Attempts to model this with a third or fourth cumulant improved data reproduction but obtained physically-implausible oxygen coordination numbers (e.g., 3±1). Structural model fitting with a split oxygen shell reproduced the data well (Figure 6), obtaining a total coordination number of ~8 with an average Yb-O distance of ~2.36 Å (Table S2). There were no statistically significant differences in fitting parameters induced by a decrease in ionic strength from 0.01 M to 0.001 M (Table S2). The relatively ordered Yb-O shells (Table S2), lack of substantial second-shell features, and substantial oscillations in the spectra beyond k = 10 Å-1 (Figure 6) are consistent with outer-sphere adsorption, in agreement with the observed effects of electrolyte concentration on macroscopic adsorption (Figure 2).

Increasing the pH to 6 and 7 weakened the EXAFS oscillations beyond k = 9 $Å^{-1}$ (Figure 6), suggesting an increase in disorder. Application of a similar structural model obtained similar total coordination but required a substantially increased σ^2, confirming that the oxygen coordination shell becomes more disordered, i.e., there is a wider distribution of Yb-O bond lengths. These changes indicate a transition in the adsorption mechanism as pH increased, with the greater disorder at pH 6 and 7 consistent with the formation of inner-sphere complexes because bonding to a surface functional group should distort the first coordination shell. The addition of an aluminum or silicon neighbor to the structural model increased the χ_v^2 value and yielded a

coordination number within the error of zero, both indicators that this change did not statistically improve the fit and is thus unjustified. This does not preclude the presence of such neighbors, but the weak backscattering from such atoms and the likely disordered nature of Yb-Al/Si interatomic distances would make their spectral contribution unobservable above the noise level in the data.

The addition of citrate had a distinct impact on the EXAFS spectra at pH 3.5 and 7. At the lower pH value, the spectrum was essentially identical to the spectra without citrate at pH 3.5 and 4 (Figure 6). The structural model fitting parameters did not display a statistically significant change upon citrate addition (Table S2), indicating that the first coordination shell is unperturbed and that citrate is likely not coordinated to adsorbed Yb at this pH value. In contrast, the EXAFS oscillations in the high k region differ in the absence and presence of citrate at pH 7 (Figure 6). This may indicate the formation of a Yb-citrate ternary surface complex. The low Yb surface coverage with citrate present resulted in substantial noise, and it is not possible to determine if citrate is directly coordinated to Yb.

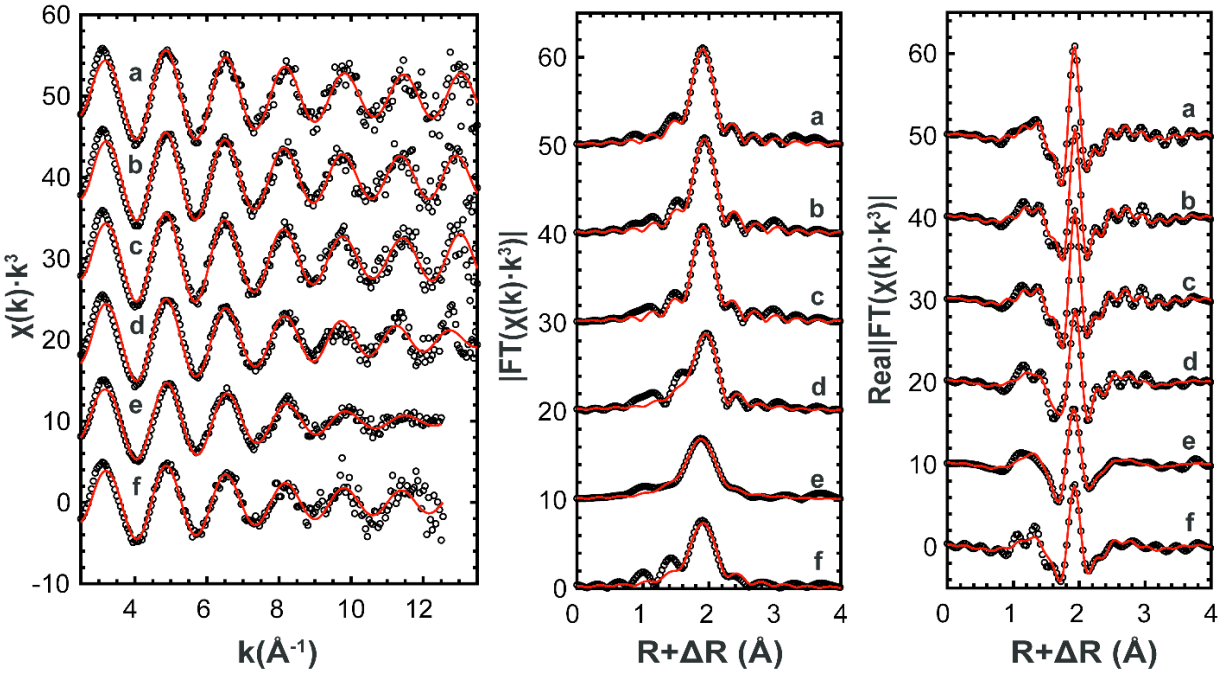

Figure 6. The L_3-edge EXAFS spectra (left) and corresponding Fourier transform magnitudes (center) and real components (right) of Yb adsorbed to kaolinite: (a) 100 µM citrate, 10 mM NaCl, pH 3.5; (b) 10 mM NaCl, pH 3.5; (c) 1 mM NaCl, pH 4; (d) 10 mM NaCl, pH 6; (e) 10 mM NaCl, pH 7; (f) 100 µM citrate, 10 mM NaCl, pH 7. Total REE concentration was 10 µM Yb and kaolinite loading was 0.2 g/L in all experiments. The solutions in all experiments were in equilibrium with atmospheric CO_2. The data (black symbols) were fitted with a FEFF-based structure model (red lines). Fitting parameters are listed in Table S2.

Development of the surface complexation model

The model features two mechanisms, ion exchange and surface complexation to edge sites, to capture retention trends at both low and high pH values. The dependence of REE adsorption on electrolyte type and concentration at pH < ~6 and the ordered first oxygen shell coordinating to Yb at pH 3.5 and 4 identified by EXAFS spectroscopy suggest that cation exchange is the dominant binding mechanism at low pH values. Therefore, Gaines-Thomas coefficients for ion exchange reactions were optimized to fit adsorption data at pH < 4.5, where ion exchange is dominant, and any contributions to adsorption to edge sites are minimal. At higher pH values, a weaker dependance of REE adsorption on electrolyte type and concentration and the distortion of the first coordination shell of Yb observed by EXAFS measurements indicate a transition to binding via inner-sphere surface complexation. The stoichiometry of surface complexes, however, cannot be resolved based on EXAFS spectroscopy alone since EXAFS spectroscopy was unable to provide substantial constraints. Therefore, we adhered to a "parsimony principle", which favors a simpler model with the smallest number of adjustable parameters needed to capture the adsorption trends over a wide range of water chemistry conditions.[64]

Surface complexation to edge sites was interpreted with the diffuse double-layer model (DLM) by including two surface complexes ($\equiv SOREE^{2+}$ and $\equiv SOREEOH^{+}$) representing the simplest stoichiometry. We used the entire dataset containing all pH values to optimize the equilibrium constants of these two surface complexes and included ion exchange reactions. The optimized

Gaines-Thomas coefficients were fixed from the previous step. The fitting of titration data (Figure S13) provided the deprotonation constant of kaolinite edge sites. One deprotonation constant and a single site type (≡S) were enough to obtain a satisfactory fit for titration ($R^2 > 0.9$). Data points at which thermodynamic calculations predict precipitation of REEs (mostly pH > ~7 and 10 μM total REE concentration) were not included in the optimization. The adsorption of REEs in the presence of LMWOAs (citric and oxalic acids) was first modeled by considering only binary (organic ligand-kaolinite and REE-kaolinite separately) surface complexation reactions, which assumes that REEs and LMWOAs adsorb to kaolinite separately. In the case of the unsatisfactory fit with the system of binary interactions, ternary surface complexes were added. Ternary surface complexes include LMWOAs as components in addition to REE^{3+}, H^+, and kaolinite surface sites. The detailed procedure describing the development of SCM can be found in the supporting information.

Surface complexation model

The fitted Gaines-Thomas coefficients (Table 1) successfully described adsorption trends at lower pH values (Figures 1-7). Modeling suggests that ion exchange is an important adsorption mechanism not only at low pH values but also at pH values up to 6-7, depending on water chemistry conditions. Model fits for the three REEs (10 μM) in the presence of 10 mM NaCl (Figures 7A-C) show that ion exchange dominates adsorption up to pH 6.5 (Nd), 6.3 (Dy), and 6.1 (Yb). Adsorption of 1 μM Nd in the presence of 1 mM NaCl can be entirely due to ion exchange up to pH 8 (Figure 7D). In the presence of 10 mM NaCl and 1 μM Yb, ion exchange is dominant up to pH 6.5 (Figure 7E). Our model suggests that, despite natural kaolinite's low CEC among clays, ion exchange is still an extremely important adsorption mechanism for REEs.

Table 1. Optimized Gaines-Thomas coefficients (K_{GT}) for ion exchange.

Ion exchange reactions	Log K_{GT}[a]
$\equiv X^-H^+ + Na^+ \rightleftharpoons \equiv X^-Na^+ + H^+$	-2.3
$2\equiv X^-H^+ + Ca^{2+} \rightleftharpoons 2(\equiv X^-)Ca^{2+} + 2H^+$	-2.2
$3\equiv X^-H^+ + Nd^{3+} \rightleftharpoons 3(\equiv X^-)Nd^{3+} + 3H^+$	-1.6
$3\equiv X^-H^+ + Dy^{3+} \rightleftharpoons 3(\equiv X^-)Dy^{3+} + 3H^+$	-1.7
$3\equiv X^-H^+ + Yb^{3+} \rightleftharpoons 3(\equiv X^-)Yb^{3+} + 3H^+$	-1.6

[a]The activity of a surface complex in K_{GT} is expressed as a surface coverage fraction. The total site concentration for ion exchange sites (≡X) is the CEC (22.5 meq/kg).

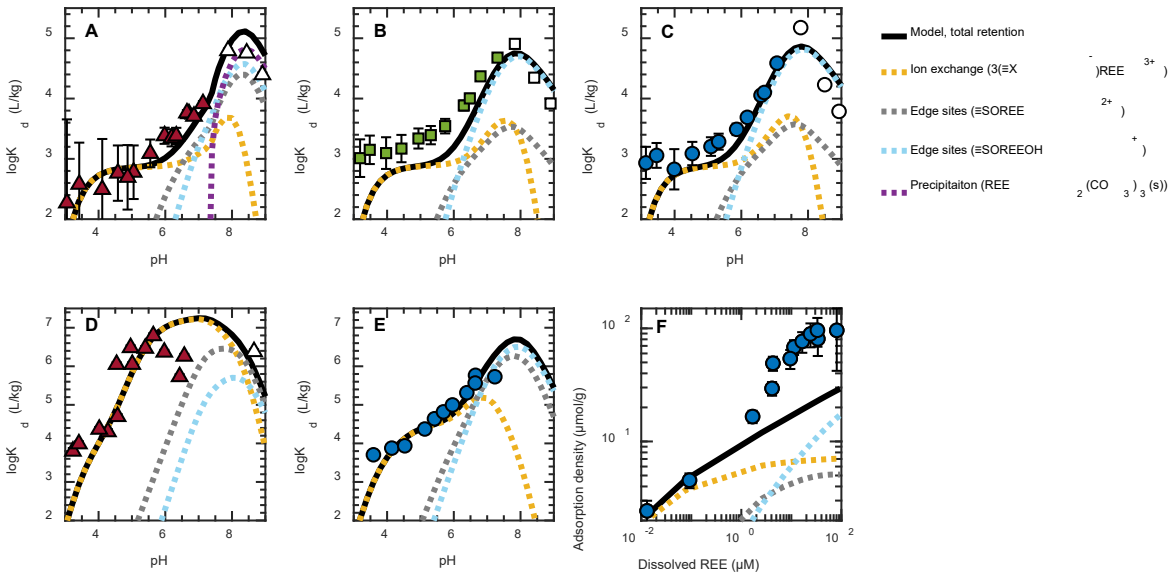

Figure 7. Detailed overview of the output of SCM (lines) in selected experiments. Markers represent retention of (A) 10 µM Nd, (B) 10 µM Dy, (C) 10 µM Yb, (D) 1 µM Nd, (E) 1 µM Yb, (F) 0.1-100 µM Yb to kaolinite (0.2 g/L). DIC in all experiments was in equilibrium with atmospheric CO_2. The electrolyte was 10 mM NaCl in all panels, except (D), where NaCl concentration was 1 mM. White markers show data points at which solubility calculations predict REE precipitation.

The fitted equilibrium constants (logK) (Table 2) successfully captured almost all adsorption trends at pH above 6 (Figures 1-7). The full adsorption dataset with the corresponding model fits can be found in the supplementary information (Figures S15-S18). Adsorption to edge sites becomes important at medium to high pH values (> 6) and at higher total REE concentrations. The model did not predict precipitation of Dy- and Yb-containing solids at high pH values (even if data are above solubility limits for kaolinite-free solubility calculations in Figure S3, indicated by white

markers). The model predicted that adsorption to kaolinite caused the dissolved REE concentrations to drop below solubility limits. Overall, the observations and model suggest that adsorption alone is responsible for the observed retention of Dy and Yb. At pH > 8, carbonate ligands form aqueous complexes with Dy and Yb, decreasing the adsorption above pH 8 (Figures 1 and 7B-C). Nd, however, is predicted to precipitate as $Nd_2(CO_3)_3(s)$ above pH 7.4 by the SCM when the Nd concentration is 10 μM (Figure 7A), in agreement with solubility calculations. In Figure 3, the convergence of all modeled adsorption edges into one line at pH > 7.5 indicates that the model predicts Nd precipitation at pH > 7.5. Adsorption of Nd to edge sites is generally weak and dominant only in a narrow pH range (6.5-7.4), leaving ion exchange and precipitation as the main retention mechanisms at low and high pH values, respectively. Lighter REEs are more prone to precipitation at high pH values (> 7) than heavier REEs, possibly explaining their enrichment in carbonatite deposits.[65] The model did not require the addition of ternary surface complexes (REE-carbonate-kaolinite) to provide satisfactory fits of the experimental data in the presence of LMWOAs.

Table 2. Optimized DLM equilibrium constants describing adsorption to edge sites.

Surface reactions	logK[a]
Deprotonation of edge sites[b]	
$\equiv SOH \rightleftharpoons \equiv SO^- + H^+$	-5.7
Adsorption of LMWOAs to edge sites[c]	
$\equiv SOH + Citrate^{3-} \rightleftharpoons \equiv SOHCitrate^{3-}$	11.1
$\equiv SOH + Citrate^{3-} + H^+ \rightleftharpoons \equiv SOHHCitrate^{2-}$	13.5
$\equiv SOH + Oxalate^{2-} \rightleftharpoons \equiv SOHOxalate^{2-}$	7.6
Adsorption of REEs to edge sites	
$\equiv SOH + Nd^{3+} \rightleftharpoons \equiv SONd^{2+} + H^+$	-5.5
$\equiv SOH + Dy^{3+} \rightleftharpoons \equiv SODy^{2+} + H^+$	-4.5
$\equiv SOH + Yb^{3+} \rightleftharpoons \equiv SOYb^{2+} + H^+$	-3.9
$\equiv SOH + Nd^{3+} + H_2O \rightleftharpoons \equiv SONdOH^+ + 2H^+$	-11.2
$\equiv SOH + Dy^{3+} + H_2O \rightleftharpoons \equiv SODyOH^+ + 2H^+$	-9.5
$\equiv SOH + Yb^{3+} + H_2O \rightleftharpoons \equiv SOYbOH^+ + 2H^+$	-8.9

[a]Activity of a surface complex in intrinsic equilibrium constants describing complexation to edge sites is expressed as a mole fraction. The site density of edge sites (≡S) was assumed to be 8.2 nm^-

^{2} based on edge surface area (assuming that edge sites make up 40% of BET surface area or 8.6 m^2/g). [b]Details of the fitting are in the supporting information. [c]The dataset used to optimize equilibrium constants describing the adsorption of LMWOAs to kaolinite (in the absence of REEs) was obtained from previous studies. More details can be found in the supplementary information (section titled "The detailed development of SCM"). All other equilibrium constants were optimized based on adsorption data from this study.[57,66]

Equilibrium constants (logK) of surface complexes correlate well with stability constants of $REEOH^+$ (Figure 8) and ionic radii of REEs (Figure S19). As REEs become heavier, more prone to hydrolysis,[67] and smaller in their ionic radii, equilibrium constants for both surface complexes increase, indicating that the adsorption strength follows the order of Yb > Dy > Nd. This finding agrees with the observation that IADs are selective for heavy REEs compared to other deposit types.[14,16] Heavy REEs that form stronger complexes with aqueous hydroxyl species also form stronger complexes with surface hydroxyl species.

After finding the equilibrium constants resulting in the minimum RSS (markers in Figure 8), we performed a sensitivity analysis to determine the range of equilibrium constant values that would keep the RSS within 5% of its minimum value (uncertainty bars in Figure 8). The optimized logK values of Dy- and Yb-associated surface complexes vary by ± 0.4, whereas that of $\equiv SONd^{2+}$ varies by ± 0.8 units. Uncertainty bars of $\equiv SONdOH^+$ extend to negative infinity, indicating that Nd adsorption could be described with only $\equiv SONd^{2+}$ because removing $\equiv SONdOH^+$ from the model does not increase the minimum RSS by more than 5% (Figure 8B). The sensitivity analysis suggests that hydrolyzed Nd surface complexes are unlikely on kaolinite's edge sites, which is in agreement with the weak hydrolysis of lighter REEs.

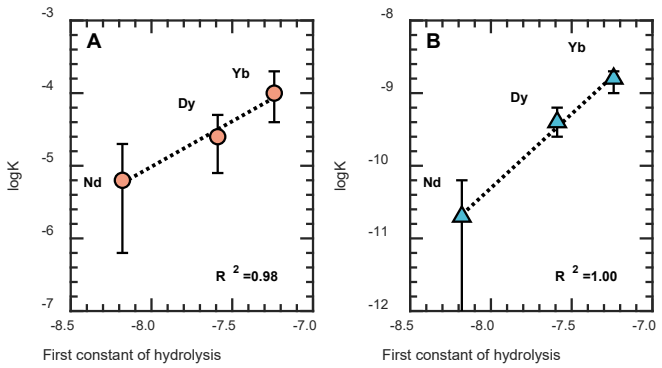

Figure 8. Equilibrium constants for adsorption reactions on edge sites in DLM for (A) ≡SOREE^{2+} and (B) ≡SOREEOH^{+} surface complexes as a function of the first stability constant of hydrolysis (REEOH^{+}). The stability constants of hydrolysis were taken from Table S1. Markers represent the fitted equilibrium constants, whereas dotted lines represent the linear function fitting. Error bars represent the range of equilibrium constants that result in RSS within 5% of the minimum RSS.

IADs are more acidic (pH 4-5) near the upper portions of the deposits, where ion exchange is likely the main mechanism governing REE retention.[68] Lower depths of REE enrichment zones are less acidic and can have pH values of up to ~6-7, depending on the location of IADs.[13,14,68] The increase in pH suggests a higher contribution of edge sites to the overall adsorption, but ion exchange can still be important depending on the electrolyte and the kaolinite CEC. This study suggests that both ion exchange and inner-sphere adsorption to edge sites contribute to REE retention at pH values relevant to the enrichment zones. Ion exchange coefficients do not show preference towards any REE, whereas equilibrium constants for inner-sphere surface complexation to edge sites are higher for heavy REEs. Therefore, the complexation to edge sites of kaolinite might be responsible for the observed relative enrichment of heavy REEs in the kaolinite-rich IADs.

To model experiments containing citric acid, we used a model in which REEs and citric acid adsorb to kaolinite separately (Figure 5 and Figure S20). The model resulted in a satisfactory fit at pH > 6 since the calculated adsorption was within the uncertainty bars of the data. However, at pH < 6, the SCM with only binary reactions underestimated adsorption. The inclusion of ternary surface complexes (REE-citric acid-kaolinite) can improve the fit at pH < 6 substantially (Figure S20);

however, EXAFS did not observe any difference between spectra with or without citric acid at pH 3.5 and 4 that would have been indicative of REE-citric acid-kaolinite ternary surface complexes. Therefore, we did not include ternary complexes in the model to align it with spectroscopic evidence.

Modeling adsorption in the presence of oxalic acid with only binary reactions underpredicted REE adsorption substantially (Figure S21). To match the experimental data and the modeled adsorption, the inclusion of ternary surface complexes was necessary (Figure S21). The evidence of ternary complexes (REE-oxalic acid-kaolinite) in the oxalic acid-containing system is based on surface complexation modeling (more details can be found in the supporting information).

We applied the model to predict adsorption in the mixed batch experiments, which were excluded from the dataset used for the optimization of equilibrium constants to evaluate the performance of the model. The model predicts lower adsorption in the mixed batch experiments compared to the separate batch experiments, in agreement with the experimental data (Figure S18). Competition between REEs for the limited availability of adsorption sites (4.5 μeq/L ion exchange sites and 23 μM edge sites at 0.2 g/L kaolinite) is responsible for the decreased adsorption. Although the model overpredicts the Dy and Yb adsorption in 1 μM mixed batch experiments at pH > 7, the model fits are mostly within the uncertainty bars of the data, indicating that overall, the model captured the effect of the competition among REEs.

Modeling adsorption to edge sites with DLM provided satisfactory model fits for all the adsorption data except for the isotherm experiments at pH 6 (Figures 4 and 7F). The poor DLM fit is attributed to the effect of electrostatic interactions because the adsorption of REEs as $\equiv SOREE^{2+}$ and $\equiv SOREEOH^{+}$ increases the surface charge of edge sites, making the surface potential more

positive and limiting further adsorption of REE^{3+}. To examine how the electrostatic term affects the adsorption, we implemented an alternative non-electrostatic model (NEM). The NEM was optimized in the same way as the DLM and based on the same dataset. The supplementary information file provides details about the development of the NEM. Unlike DLM, the development of NEM required the addition of two surface sites. The NEM predicted adsorption at high REE concentrations in the isotherms well, but it provided a poor fit of the adsorption data with 1 μM total REE concentrations at pH > 7 (Figure S23-S27) and some adsorption data in the presence of $CaCl_2$ (Figure S25B and S25E), contrasting the excellent performance of the DLM at these water chemistry conditions. The electrostatic term in the DLM is necessary for modeling the effects of pH and ligands on adsorption, but the DLM's electrostatic term failed to describe experiments involving high loadings of REEs. Neither DLM nor NEM can fully describe adsorption trends for all water chemistry conditions, which points to a need to re-visit the formulation of a diffuse layer model for clay minerals. Previous studies on montmorillonite noted that negative charge from basal surfaces spills over to edge sites.[69,70] Including the spillover effect for the classic DLM would render surface potential more negative, increasing the affinity for REE adsorption. The predicted REE adsorption densities in the isotherm experiments would increase if such a spillover effect had been included in the current model for kaolinite. However, the extent of the increase in the REE adsorption might not be enough to account for the observed difference since kaolinite's CEC (20-30 meq/kg) is considerably smaller than that of montmorillonite (700-800 meq/kg).[28] Another possible reason for the underestimation of isotherm might be the formation of polynuclear surface complexes at high REE loadings that are not considered in the current model. Such polynuclear surface complexes have been suggested in a previous study of Eu uptake by kaolinite.[22]

Conclusions

This study sought to expand current knowledge of REE mobility and retention in subsurface environments abundant in clay minerals such as kaolinite with batch adsorption experiments covering a wide range of experimental conditions (pH, DIC, total REE concentration, and LMWOAs), SCM, and EXAFS spectroscopy. Our results demonstrate that water chemistry changes the binding mechanism of REEs to kaolinite. In acidic environments (pH 3-5), ion exchange on basal planes is the dominant adsorption mechanism despite the low cation exchange capacity of natural kaolinites. Ion exchange can be the main adsorption mode at pH values up to 7-8 when concentrations of electrolyte and REEs are low. At higher pH values (> 6), surface complexation to edge sites becomes more important than ion exchange. The SCM found higher equilibrium constants for heavy REEs, indicating affinity in the order of Yb > Dy > Nd. These findings are helpful for understanding the formation of IADs and improving existing recovery strategies by providing insights into the adsorption mechanism. The REE recovery method used for ion adsorption deposits uses an ammonium sulfate solution at pH 3-4 to extract REEs via ion exchange.[71] One implication of the model is that increasing the pH value of the extraction will limit the recovery of REEs. At higher pH values, REEs form inner-sphere complexes and are unlikely to be displaced by a weakly sorbing ion such as NH_4^+.

DIC is the primary factor affecting adsorption at pH > 8 because it can separate light REEs from heavy REEs by precipitation. At pH > 8, DIC forms strong aqueous complexes with heavy REEs, limiting their adsorption. High-pH environments will promote the mobility of heavy REEs but will be enriched with light REEs in a precipitated form. Although groundwater pH levels within IADs are below pH 8, this finding is relevant to other systems, such as alkaline hot springs.[72]

642 The SCM captured the main adsorption trends with ion exchange and the inner-sphere
643 complexation, and EXAFS spectra supported the predicted trends in binding mechanisms.
644 Modeling enables understanding of REE behavior in subsurface environments subject to ionic
645 strength and pH conditions beyond those studied in experiments. SCM indicated the presence of
646 ternary surface complexes (REE-oxalic acid-kaolinite) in oxalate-containing systems. The
647 combination of SCM and EXAFS suggested that ternary surface complexes do not form with
648 REEs, kaolinite, and citric acid, although such ternary surface complexes cannot be ruled out. The
649 SCM should be used with caution when applied to predict the adsorption of high REE
650 concentrations to kaolinite since the model underestimated the adsorption of REE concentrations
651 above 25 μM. The model advances the predictive ability to estimate REE concentrations in the
652 environment regardless of whether REEs are viewed as a resource or as a contaminant. The SCM
653 can be used in reactive transport models to advance understanding of the fate and transport of REE
654 and possibly other trivalent cations.

655

656

657

Supporting information

The supporting information file contains information about the SEM image of kaolinite particles, a summary of cleaning and fractionation procedures, calculation of uncertainty bars, stability constants for aqueous complexes with REEs with speciation and solubility diagrams, supporting figures, all figures from the Results and Discussion re-plotted on %adsorbed scale, structural model fitting results for the EXAFS, the detailed description of model development, the results from potentiometric titration, all experimental data with the associated surface complexation model (DLM) outputs, the description of modeling the effect of oxalic acid on adsorption of Dy and Yb, detailed overview of the non-electrostatic model, and all experimental data with the associated surface complexation model (NEM) outputs. The supporting figures show the effect of the total REE concentration, adsorption of REEs in the mixed batch, the effect of oxalic acid on REE adsorption, and equilibrium constants for adsorption reactions plotted against ionic radii.

Acknowledgments

This project was supported by the U.S. Department of Energy, Office of Science, Office of Basic Energy Sciences, Critical Minerals and Materials program under Award Number DE-SC0022213. The authors thank collaborators Eugene Ilton, Eric Bylaska, and Sebastian Mergelsberg at the Pacific Northwest National Laboratory. ICP-MS and BET surface area analyzer from the Chemical and Environmental Analysis Facility (CEAF) at Washington University in St. Louis were used in this study. Use of the Stanford Synchrotron Radiation Lightsource, SLAC National Accelerator Laboratory, is supported by the U.S. Department of Energy, Office of Science, Office of Basic Energy Sciences under Contract No. DE-AC02-76SF00515. The authors acknowledge financial support from Washington University in St. Louis and the Institute of Materials Science and Engineering for the use of instruments and staff assistance. The authors thank Xueyi Liu for assistance in some experiments examining the effect of electrolyte concentration on REE adsorption at pH 4. The authors thank Sandra Matteucci for her assistance with revising the manuscript.

References

(1) Zhou, J.; Fiete, G. A. Rare Earths in a Nutshell. *Physics Today* **2020**, *73* (1), 66–67. https://doi.org/10.1063/PT.3.4397.

(2) Dushyantha, N.; Batapola, N.; Ilankoon, I. M. S. K.; Rohitha, S.; Premasiri, R.; Abeysinghe, B.; Ratnayake, N.; Dissanayake, K. The Story of Rare Earth Elements (REEs): Occurrences, Global Distribution, Genesis, Geology, Mineralogy and Global Production. *Ore Geology Reviews* **2020**, *122*, 103521. https://doi.org/10.1016/j.oregeorev.2020.103521.

(3) Dutta, T.; Kim, K.-H.; Uchimiya, M.; Kwon, E. E.; Jeon, B.-H.; Deep, A.; Yun, S.-T. Global Demand for Rare Earth Resources and Strategies for Green Mining. *Environmental Research* **2016**, *150*, 182–190. https://doi.org/10.1016/j.envres.2016.05.052.

(4) Fujita, Y.; McCall, S. K.; Ginosar, D. Recycling Rare Earths: Perspectives and Recent Advances. *MRS Bulletin* **2022**, *47* (3), 283–288. https://doi.org/10.1557/s43577-022-00301-w.

(5) Jowitt, S. M. Mineral Economics of the Rare-Earth Elements. *MRS Bulletin* **2022**, *47* (3), 276–282. https://doi.org/10.1557/s43577-022-00289-3.

(6) Alshameri, A.; He, H.; Xin, C.; Zhu, J.; Xinghu, W.; Zhu, R.; Wang, H. Understanding the Role of Natural Clay Minerals as Effective Adsorbents and Alternative Source of Rare Earth Elements: Adsorption Operative Parameters. *Hydrometallurgy* **2019**, *185*, 149–161. https://doi.org/10.1016/j.hydromet.2019.02.016.

(7) Reich, M.; Simon, A. C. Critical Minerals. *Annual Review of Earth and Planetary Sciences* **2024**. https://doi.org/10.1146/annurev-earth-040523-023316.

(8) Chen, P.; Ilton, E. S.; Wang, Z.; Rosso, K. M.; Zhang, X. Global Rare Earth Element Resources: A Concise Review. *Applied Geochemistry* **2024**, 106158. https://doi.org/10.1016/j.apgeochem.2024.106158.

(9) Moldoveanu, G. A.; Papangelakis, V. G. An Overview of Rare-Earth Recovery by Ion-Exchange Leaching from Ion-Adsorption Clays of Various Origins. *Mineral. mag.* **2016**, *80* (1), 63–76. https://doi.org/10.1180/minmag.2016.080.051.

(10) Wu, Z.; Chen, Y.; Wang, Y.; Xu, Y.; Lin, Z.; Liang, X.; Cheng, H. Review of Rare Earth Element (REE) Adsorption on and Desorption from Clay Minerals: Application to Formation and Mining of Ion-Adsorption REE Deposits. *Ore Geology Reviews* **2023**, *157*, 105446. https://doi.org/10.1016/j.oregeorev.2023.105446.

(11) He, Y.; Ma, L.; Li, X.; Wang, H.; Liang, X.; Zhu, J.; He, H. Mobilization and Fractionation of Rare Earth Elements during Experimental Bio-Weathering of Granites. *Geochimica et Cosmochimica Acta* **2023**, *343*, 384–395. https://doi.org/10.1016/j.gca.2022.12.027.

(12) Sanematsu, K.; Watanabe, Y. Characteristics and Genesis of Ion Adsorption-Type Rare Earth Element Deposits. In *Rare Earth and Critical Elements in Ore Deposits*; Society of Economic Geologists, 2016. https://doi.org/10.5382/Rev.18.03.

(13) Nagasawa, M.; Shimizu, Y.; Yamaguchi, A.; Tokunaga, K.; Mukai, H.; Aoyagi, N.; Mei, H.; Takahashi, Y. Interpretation of Vertical Migration and Enrichment Processes of Rare Earth Elements (REEs) in Ion-Adsorption-Type Mineralization in Japan Based on REE Speciation Analyses. *Chemical Geology* **2024**, *670*, 122431. https://doi.org/10.1016/j.chemgeo.2024.122431.

(14) Borst, A. M.; Smith, M. P.; Finch, A. A.; Estrade, G.; Villanova-de-Benavent, C.; Nason, P.; Marquis, E.; Horsburgh, N. J.; Goodenough, K. M.; Xu, C.; Kynický, J.; Geraki, K.

Adsorption of Rare Earth Elements in Regolith-Hosted Clay Deposits. *Nat Commun* **2020**, *11* (1), 4386. https://doi.org/10.1038/s41467-020-17801-5.
(15) Li, M. Y. H.; Zhou, M.-F.; Williams-Jones, A. E. Controls on the Dynamics of Rare Earth Elements During Subtropical Hillslope Processes and Formation of Regolith-Hosted Deposits. *Economic Geology* **2020**, *115* (5), 1097–1118. https://doi.org/10.5382/econgeo.4727.
(16) Yang, M.; Liang, X.; Ma, L.; Huang, J.; He, H.; Zhu, J. Adsorption of REEs on Kaolinite and Halloysite: A Link to the REE Distribution on Clays in the Weathering Crust of Granite. *Chemical Geology* **2019**, *525*, 210–217. https://doi.org/10.1016/j.chemgeo.2019.07.024.
(17) Zhou, J.; Liu, H.; Liu, D.; Yuan, P.; Bu, H.; Du, P.; Fan, W.; Li, M. Sorption/Desorption of Eu(III) on Halloysite and Kaolinite. *Applied Clay Science* **2022**, *216*, 106356. https://doi.org/10.1016/j.clay.2021.106356.
(18) Jo, J.; Yamanaka, T.; Shin, D. Nitrogen Isotope Geochemistry of Ion Adsorption-Type REE Mineralization: Insights from the Weathered Granitoid Rocks in the Sancheong District, South Korea. *Ore Geology Reviews* **2023**, *157*, 105429. https://doi.org/10.1016/j.oregeorev.2023.105429.
(19) Tournassat, C.; Bourg, I. C.; Steefel, C. I.; Bergaya, F. Surface Properties of Clay Minerals. In *Developments in Clay Science*; Elsevier, 2015; Vol. 6, pp 5–31. https://doi.org/10.1016/B978-0-08-100027-4.00001-2.
(20) Kang, M. J.; Hahn, P. S. Adsorption Behavior of Aqueous Europium on Kaolinite under Various Disposal Conditions. *Korean J. Chem. Eng.* **2004**, *21* (2), 419–424. https://doi.org/10.1007/BF02705430.
(21) Coppin, F.; Berger, G.; Bauer, A.; Castet, S.; Loubet, M. Sorption of Lanthanides on Smectite and Kaolinite. *Chemical Geology* **2002**, *182* (1), 57–68. https://doi.org/10.1016/S0009-2541(01)00283-2.
(22) Ishida, K.; Saito, T.; Aoyagi, N.; Kimura, T.; Nagaishi, R.; Nagasaki, S.; Tanaka, S. Surface Speciation of Eu3+ Adsorbed on Kaolinite by Time-Resolved Laser Fluorescence Spectroscopy (TRLFS) and Parallel Factor Analysis (PARAFAC). *Journal of Colloid and Interface Science* **2012**, *374* (1), 258–266. https://doi.org/10.1016/j.jcis.2012.01.060.
(23) Stumpf, T.; Bauer, A.; Coppin, F.; Fanghänel, T.; Kim, J.-I. Inner-Sphere, Outer-Sphere and Ternary Surface Complexes: A TRLFS Study of the Sorption Process of Eu(III) onto Smectite and Kaolinite. *Radiochimica Acta* **2002**, *90* (6), 345–349. https://doi.org/10.1524/ract.2002.90.6.345.
(24) Tertre, E.; Berger, G.; Simoni, E.; Castet, S.; Giffaut, E.; Loubet, M.; Catalette, H. Europium Retention onto Clay Minerals from 25 to 150°C: Experimental Measurements, Spectroscopic Features and Sorption Modelling. *Geochimica et Cosmochimica Acta* **2006**, *70* (18), 4563–4578. https://doi.org/10.1016/j.gca.2006.06.1568.
(25) Sugiura, Y.; Ishidera, T.; Aoyagi, N.; Mei, H.; Saito, T.; Tachi, Y. Trivalent Lanthanide Sorption onto Illite in the Presence of Carbonate: A Study Combining Thermodynamic Sorption Modeling, Time-Resolved Laser Fluorescence Spectroscopy, and Parallel Factor Analysis. *Applied Clay Science* **2024**, *258*, 107476. https://doi.org/10.1016/j.clay.2024.107476.
(26) Gu, Q.; Liu, J.; Yang, Y.; Zhu, R.; Ma, L.; Liang, X.; Long, S.; Zhu, J.; He, H. The Different Effects of Sulfate on the Adsorption of REEs on Kaolinite and Ferrihydrite. *Applied Clay Science* **2022**, *221*, 106468. https://doi.org/10.1016/j.clay.2022.106468.

(27) Ganor, J.; Reznik, I. J.; Rosenberg, Y. O. Organics in Water-Rock Interactions. *Reviews in Mineralogy and Geochemistry* **2009**, *70* (1), 259–369. https://doi.org/10.2138/rmg.2009.70.7.
(28) Liu, X.-R.; Liu, W.-S.; Tang, Y.-T.; Wang, S.-Z.; Cao, Y.-J.; Chen, Z.-W.; Xie, C.-D.; Liu, C.; Guo, M.-N.; Qiu, R.-L. Effects of in Situ Leaching on the Origin and Migration of Rare Earth Elements in Aqueous Systems of South China: Insights Based on REE Patterns, and Ce and Eu Anomalies. *Journal of Hazardous Materials* **2022**, *435*, 128959. https://doi.org/10.1016/j.jhazmat.2022.128959.
(29) Wan, Y.; Liu, C. The Effect of Humic Acid on the Adsorption of REEs on Kaolin. *Colloids and Surfaces A: Physicochemical and Engineering Aspects* **2006**, *290* (1), 112–117. https://doi.org/10.1016/j.colsurfa.2006.05.010.
(30) Takahashi, Y.; Minai, Y.; Ambe, S.; Makide, Y.; Ambe, F. Comparison of Adsorption Behavior of Multiple Inorganic Ions on Kaolinite and Silica in the Presence of Humic Acid Using the Multitracer Technique. *Geochimica et Cosmochimica Acta* **1999**, *63* (6), 815–836. https://doi.org/10.1016/S0016-7037(99)00065-4.
(31) Flynn, E. D.; Catalano, J. G. Influence of Oxalate on Ni Fate during Fe(II)-Catalyzed Recrystallization of Hematite and Goethite. *Environ. Sci. Technol.* **2018**, *52* (12), 6920–6927. https://doi.org/10.1021/acs.est.8b00641.
(32) Yang, X. J.; Lin, A.; Li, X.-L.; Wu, Y.; Zhou, W.; Chen, Z. China's Ion-Adsorption Rare Earth Resources, Mining Consequences and Preservation. *Environmental Development* **2013**, *8*, 131–136. https://doi.org/10.1016/j.envdev.2013.03.006.
(33) Bishop, B. A.; Alam, Md. S.; Flynn, S. L.; Chen, N.; Hao, W.; Ramachandran Shivakumar, K.; Swaren, L.; Gutierrez Rueda, D.; Konhauser, K. O.; Alessi, D. S.; Robbins, L. J. Rare Earth Element Adsorption to Clay Minerals: Mechanistic Insights and Implications for Recovery from Secondary Sources. *Environ. Sci. Technol.* **2024**, acs.est.4c00974. https://doi.org/10.1021/acs.est.4c00974.
(34) Bradbury, M. H.; Baeyens, B. Sorption of Eu on Na- and Ca-Montmorillonites: Experimental Investigations and Modelling with Cation Exchange and Surface Complexation. *Geochimica et Cosmochimica Acta* **2002**, *66* (13), 2325–2334. https://doi.org/10.1016/S0016-7037(02)00841-4.
(35) Kulik, D. A.; Aja, S. U.; Sinitsyn, V. A.; Wood, S. A. Acid–Base Surface Chemistry and Sorption of Some Lanthanides on K+-Saturated Marblehead Illite: II. a Multisite–Surface Complexation Modeling. *Geochimica et Cosmochimica Acta* **2000**, *64* (2), 195–213. https://doi.org/10.1016/S0016-7037(99)00174-X.
(36) Chorover, J.; Choi, S.; Amistadi, M. K.; Karthikeyan, K. G.; Crosson, G.; Mueller, K. T. Linking Cesium and Strontium Uptake to Kaolinite Weathering in Simulated Tank Waste Leachate. *Environ Sci Technol* **2003**, *37* (10), 2200–2208. https://doi.org/10.1021/es025980x.
(37) Schroth, B. K.; Sposito, G. Surface Charge Properties of Kaolinite. *Clays Clay Miner.* **1997**, *45* (1), 85–91. https://doi.org/10.1346/CCMN.1997.0450110.
(38) Huertas, F. J.; Chou, L.; Wollast, R. Mechanism of Kaolinite Dissolution at Room Temperature and Pressure: Part 1. Surface Speciation. *Geochimica et Cosmochimica Acta* **1998**, *62* (3), 417–431. https://doi.org/10.1016/S0016-7037(97)00366-9.
(39) Ma, C.; Eggleton, R. A. Cation Exchange Capacity of Kaolinite. *Clays and Clay Minerals* **1999**, *47* (2), 174–180. https://doi.org/10.1346/CCMN.1999.0470207.

(40) Heidmann, I.; Christl, I.; Leu, C.; Kretzschmar, R. Competitive Sorption of Protons and Metal Cations onto Kaolinite: Experiments and Modeling. *Journal of Colloid and Interface Science* **2005**, *282* (2), 270–282. https://doi.org/10.1016/j.jcis.2004.08.019.
(41) Ullman, W. J.; Welch, S. A. Water-Rock Interactions, Ore Deposits, and Environmental Geochemistry: A Tribute to David A. Crerar. Organic Ligands and Feldspar Dissolution. *The Geochemical Society. Special Publication.* **2002**, *7*.
(42) Webb, S. M. SIXpack: A Graphical User Interface for XAS Analysis Using IFEFFIT. *Phys. Scr.* **2005**, No. T115, 1011. https://doi.org/10.1238/Physica.Topical.115a01011.
(43) Newville, M. IFEFFIT : Interactive XAFS Analysis and FEFF Fitting. *J Synchrotron Rad* **2001**, *8* (2), 322–324. https://doi.org/10.1107/S0909049500016964.
(44) Newville, M. Larch: An Analysis Package for XAFS and Related Spectroscopies. *J. Phys.: Conf. Ser.* **2013**, *430* (1), 012007. https://doi.org/10.1088/1742-6596/430/1/012007.
(45) Ankudinov, A. L.; Ravel, B.; Rehr, J. J.; Conradson, S. D. Real-Space Multiple-Scattering Calculation and Interpretation of x-Ray-Absorption near-Edge Structure. *Phys. Rev. B* **1998**, *58* (12), 7565–7576. https://doi.org/10.1103/PhysRevB.58.7565.
(46) Etschmann, B.; Streltsov, V.; Ishizawa, N.; Maslen, E. N. Synchrotron X-Ray Study of Er3Al5O12 and Yb3Al5O12 Garnets. *Acta Cryst B* **2001**, *57* (2), 136–141. https://doi.org/10.1107/S0108768100019923.
(47) Mermut, A. R.; Cano, A. F. Baseline Studies of the Clay Minerals Society Source Clays: Chemical Analyses of Major Elements. *Clays Clay Miner.* **2001**, *49* (5), 381–386. https://doi.org/10.1346/CCMN.2001.0490504.
(48) Kogel, J. E.; Lewis, S. A. Baseline Studies of the Clay Minerals Society Source Clays: Chemical Analysis by Inductively Coupled Plasma-Mass Spectroscopy (ICP-MS). *Clays Clay Miner.* **2001**, *49* (5), 387–392. https://doi.org/10.1346/CCMN.2001.0490505.
(49) Gustafsson, J. P. Visual MINTEQ, 2020.
(50) Xie, X.; Giammar, D. E.; Wang, Z. MINFIT: A Spreadsheet-Based Tool for Parameter Estimation in an Equilibrium Speciation Software Program. *Environ. Sci. Technol.* **2016**, *50* (20), 11112–11120. https://doi.org/10.1021/acs.est.6b03399.
(51) Liu, X.; Tournassat, C.; Grangeon, S.; Kalinichev, A. G.; Takahashi, Y.; Marques Fernandes, M. Molecular-Level Understanding of Metal Ion Retention in Clay-Rich Materials. *Nat Rev Earth Environ* **2022**, *3* (7), 461–476. https://doi.org/10.1038/s43017-022-00301-z.
(52) Ma, F.; Jin, Q.; Li, P.; Chen, Z.; Lu, J.; Guo, Z.; Wu, W. Experimental and Modelling Approaches to Am(III) and Np(V) Adsorption on the Maoming Kaolinite. *Applied Geochemistry* **2017**, *84*, 325–336. https://doi.org/10.1016/j.apgeochem.2017.07.002.
(53) Goldberg, S. Macroscopic Experimental and Modeling Evaluation of Selenite and Selenate Adsorption Mechanisms on Gibbsite. *Soil Science Society of America Journal* **2014**, *78* (2), 473–479. https://doi.org/10.2136/sssaj2013.06.0249.
(54) Borden, D.; Giese, R. F. Baseline Studies of the Clay Minerals Society Source Clays: Cation Exchange Capacity Measurements by the Ammonia-Electrode Method. *Clays Clay Miner.* **2001**, *49* (5), 444–445. https://doi.org/10.1346/CCMN.2001.0490510.
(55) Weil, R. R.; Brady, N. C. *The Nature and Properties of Soils*, 15th ed.; 2017.
(56) Li, Z.; Gallus, L. Adsorption of Dodecyl Trimethylammonium and Hexadecyl Trimethylammonium onto Kaolinite — Competitive Adsorption and Chain Length Effect. *Applied Clay Science* **2007**, *35* (3), 250–257. https://doi.org/10.1016/j.clay.2006.09.004.

(57) Lackovic, K.; Johnson, B. B.; Angove, M. J.; Wells, J. D. Modeling the Adsorption of Citric Acid onto Muloorina Illite and Related Clay Minerals. *Journal of Colloid and Interface Science* **2003**, *267* (1), 49–59. https://doi.org/10.1016/S0021-9797(03)00693-3.
(58) Ikhsan, J.; Johnson, B. B.; Wells, J. D. A Comparative Study of the Adsorption of Transition Metals on Kaolinite. *Journal of Colloid and Interface Science* **1999**, *217* (2), 403–410. https://doi.org/10.1006/jcis.1999.6377.
(59) Gu, X.; Evans, L. J. Surface Complexation Modelling of Cd(II), Cu(II), Ni(II), Pb(II) and Zn(II) Adsorption onto Kaolinite. *Geochimica et Cosmochimica Acta* **2008**, *72* (2), 267–276. https://doi.org/10.1016/j.gca.2007.09.032.
(60) Sanders, R. L.; Washton, N. M.; Mueller, K. T. Measurement of the Reactive Surface Area of Clay Minerals Using Solid-State NMR Studies of a Probe Molecule. *J. Phys. Chem. C* **2010**, *114* (12), 5491–5498. https://doi.org/10.1021/jp906132k.
(61) Brady, P. V.; Cygan, R. T.; Nagy, K. L. Molecular Controls on Kaolinite Surface Charge. *Journal of Colloid and Interface Science* **1996**, *183* (2), 356–364. https://doi.org/10.1006/jcis.1996.0557.
(62) Bickmore, B. R.; Nagy, K. L.; Sandlin, P. E.; Crater, T. S. Quantifying Surface Areas of Clays by Atomic Force Microscopy. *American Mineralogist* **2002**, *87* (5–6), 780–783. https://doi.org/10.2138/am-2002-5-622.
(63) White, G. N.; Zelazny, L. W. Analysis and Implications of the Edge Structure of Dioctahedral Phyllosilicates. *Clays Clay Miner.* **1988**, *36* (2), 141–146. https://doi.org/10.1346/CCMN.1988.0360207.
(64) Tournassat, C.; Grangeon, S.; Leroy, P.; Giffaut, E. Modeling Specific pH Dependent Sorption of Divalent Metals on Montmorillonite Surfaces. A Review of Pitfalls, Recent Achievements and Current Challenges. *American Journal of Science* **2013**, *313* (5), 395–451. https://doi.org/10.2475/05.2013.01.
(65) Song, W.; Xu, C.; Smith, M. P.; Kynicky, J.; Yang, J.; Liu, T.; Jing, D. Origin of Heavy Rare Earth Element Enrichment in Carbonatites. *Geochimica et Cosmochimica Acta* **2023**, *362*, 115–126. https://doi.org/10.1016/j.gca.2023.08.025.
(66) Ward, D. B. Effect of Al and Organic Acids on the Surface Chemistry of Kaolinite. *Clays and Clay Minerals* **1998**, *46* (4), 453–465. https://doi.org/10.1346/CCMN.1998.0460410.
(67) Bentouhami, E.; Bouet, G. M.; Meullemeestre, J.; Vierling, F.; Khan, M. A. Physicochemical Study of the Hydrolysis of Rare-Earth Elements (III) and Thorium (IV). *Comptes Rendus Chimie* **2004**, *7* (5), 537–545. https://doi.org/10.1016/j.crci.2004.01.008.
(68) Huang, J.; He, H.; Tan, W.; Liang, X.; Ma, L.; Wang, Y.; Qin, X.; Zhu, J. Groundwater Controls REE Mineralisation in the Regolith of South China. *Chemical Geology* **2021**, *577*, 120295. https://doi.org/10.1016/j.chemgeo.2021.120295.
(69) Tournassat, C.; Tinnacher, R. M.; Grangeon, S.; Davis, J. A. Modeling Uranium(VI) Adsorption onto Montmorillonite under Varying Carbonate Concentrations: A Surface Complexation Model Accounting for the Spillover Effect on Surface Potential. *Geochimica et Cosmochimica Acta* **2018**, *220*, 291–308. https://doi.org/10.1016/j.gca.2017.09.049.
(70) Tournassat, C.; Davis, J. A.; Chiaberge, C.; Grangeon, S.; Bourg, I. C. Modeling the Acid–Base Properties of Montmorillonite Edge Surfaces. *Environ. Sci. Technol.* **2016**, *50* (24), 13436–13445. https://doi.org/10.1021/acs.est.6b04677.
(71) Moldoveanu, G. A.; Papangelakis, V. G. Recovery of Rare Earth Elements Adsorbed on Clay Minerals: II. Leaching with Ammonium Sulfate. *Hydrometallurgy* **2013**, *131–132*, 158–166. https://doi.org/10.1016/j.hydromet.2012.10.011.

(72) Ge, L.; Qu, P.; Tan, H.; Xue, F. Migration and Controlling Factors of Rare Earth Elements in Geothermal Systems on the Southern Tibetan Plateau. *Chemical Geology* **2024**, 122422. https://doi.org/10.1016/j.chemgeo.2024.122422.

Adsorption of REEs to kaolinite via ion exchange and surface complexation as a function of water chemistry

Elmira Ramazanova[1], Neha Sharma[1], Elaine D. Flynn[2], Olwen Stagg[2], Jeffrey G. Catalano[2], Daniel E. Giammar[1,*]

[1]Department of Energy, Environmental and Chemical Engineering, Washington University in St. Louis, St. Louis, Missouri 63130, United States
[2]Department of Earth, Environmental, and Planetary Sciences, Washington University in St. Louis, St. Louis, Missouri 63130, United States

*Corresponding Author:
Address: Department of Energy, Environmental and Chemical Engineering, Washington University in St. Louis, St. Louis, MO 63130, USA
Phone: (314) 935-6849
Email: giammar@wustl.edu

Supporting information file for *ACS Earth and Space Chemistry.*

May 2025

Table of contents

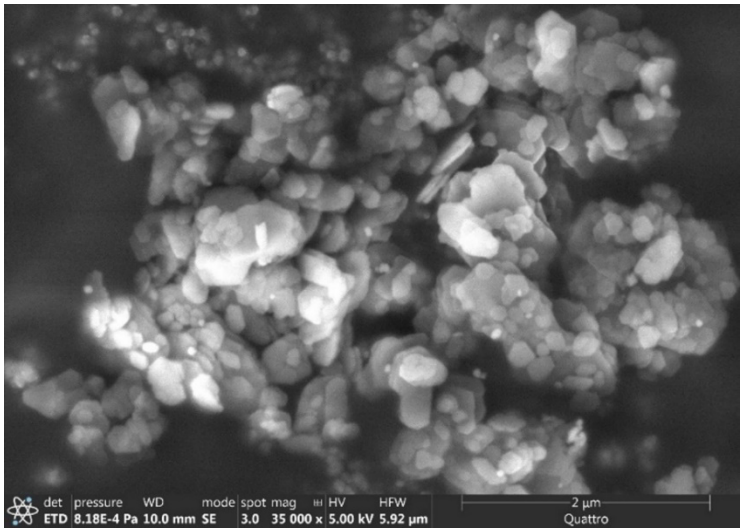

Figure S1. SEM image of kaolinite particles.

Cleaning and size fractionation of kaolinite

Kaolinite cleaning and size fractionation procedures were taken from Chorover et al.[1] Dispersion of untreated clay (30 g) in 0.01 M NaOH at pH 9.5 was followed by centrifugation (5 min at 119g) to obtain kaolinite particles with an equivalent spherical diameter of < 2 µm. Clay was resuspended and centrifuged repeatedly until the conductivity of the supernatant solution reached < 1 µS. The clay was then treated with 1 M NaCl to have Na^+-saturated clay, followed by washing with ultrapure water (18.2 MΩ·cm) water to remove residual salts. The mineral was freeze-dried and stored as a powder. New kaolinite suspension (10 g/L) was prepared from the same batch every month for batch adsorption experiments.

Calculation of uncertainties

Uncertainties of the measured concentrations (δC) from the inductively coupled plasma mass spectrometry were calculated based on the weighted calibration curve.[2] An uncertainty of 5% was assumed for dilution factors, kaolinite loading, and BET surface area. The obtained uncertainties of the measured concentration were propagated using Equations S1-S4 to calculate uncertainties of $\log K_d$ values ($\delta \log K_d$), %adsorbed values (δ(%adsorbed)), and adsorption densities (δ(Adsorption density)). C_{total} (µM) is the total concentration of REE in the reactor. $C_{supernatant}$ (µM) is the concentration measured by ICP-MS after 24 h of equilibration. C_{ads} is the adsorbed concentration (µM). $C_{kaolinite}$ (kg/L) is the kaolinite loading.

$$\delta C_{ads} = \sqrt{\delta C_{total}^2 + \delta C_{supernatant}^2} \quad \text{(Eq. S1)}$$

$$\delta \log K_d = 0.434 \sqrt{\left(\frac{\delta C_{ads}}{C_{ads}}\right)^2 + \left(\frac{\delta C_{supernatant}}{C_{supernatant}}\right)^2 + \left(\frac{\delta C_{kaolinite}}{C_{kaolinite}}\right)^2} \quad \text{(Eq. S2)}$$

$$\frac{\delta(\%\text{adsorbed})}{\%\text{adsorbed}} = 100 \sqrt{\left(\frac{\delta C_{total}}{C_{total}}\right)^2 + \left(\frac{\delta C_{ads}}{C_{ads}}\right)^2} \quad \text{(Eq. S3)}$$

$$\frac{\delta(\text{Adsorption density})}{\text{Adsorption density}} = \sqrt{\left(\frac{\delta C_{kaolinite}}{C_{kaolinite}}\right)^2 + \left(\frac{\delta C_{ads}}{C_{ads}}\right)^2} \quad \text{(Eq. S4)}$$

Table S1. Stability constants (at zero ionic strength and 25°C) of aqueous complexes and solubility products of relevant solid phases involving Nd, Dy, and Yb.

Reaction	REE			References
	Nd	Dy	Yb	
$REE^{3+} + H_2O \rightleftharpoons REEOH^{2+} + H^+$	-8.18	-7.59	-7.24	[3,4]
$REE^{3+} + 2H_2O \rightleftharpoons REE(OH)_2^+ + 2H^+$	-17.04	-16.1	-15.75	[5,6]
$REE^{3+} + 3H_2O \rightleftharpoons REE(OH)_3 + 3H^+$	-26.41	-24.4	-23.86	[5,6]
$REE^{3+} + 4H_2O \rightleftharpoons REE(OH)_4^- + 4H^+$	-37.39	-33.5	-32.7	[4,5]
$2REE^{3+} + 2H_2O \rightleftharpoons REE_2(OH)_2^{4+} + 2H^+$	-13.89			[4]
$REE^{3+} + CO_3^{2-} \rightleftharpoons REECO_3^+$	7.28	7.56	7.81	[7]
$REE^{3+} + 2CO_3^{2-} \rightleftharpoons REE(CO_3)_2^-$	12.17	12.91	13.3	[7]
$REE^{3+} + H + CO_3^- \rightleftharpoons REEHCO_3^{2+}$	12.61	12.83	12.86	[7]
$REE^{3+} + NO_3^- \rightleftharpoons REENO_3^{2+}$	0.91	0.31	0.41	[4,5,8]
$REE^{3+} + Citrate^{3-} \rightleftharpoons REECitrate^0$	9.51	9.34	9.65	[4,9]
$REE^{3+} + Oxalate^{2-} \rightleftharpoons REEOxalate^+$	6.31	6.74	6.95	[10]
$REE^{3+} + 2Oxalate^{2-} \rightleftharpoons REE(Oxalate)_2^-$	10.82	11.35	11.75	[10]
$REE^{3+} + CO_3^{2-} \rightleftharpoons REE_2(CO_3)_3$ (s)	-33	-31.5	-31.1	[4,11]
$REE^{3+} + 3H_2O \rightleftharpoons REE(OH)_3$ (s) $+ 3H^+$	18.09	16.09	15.39	[4,11]

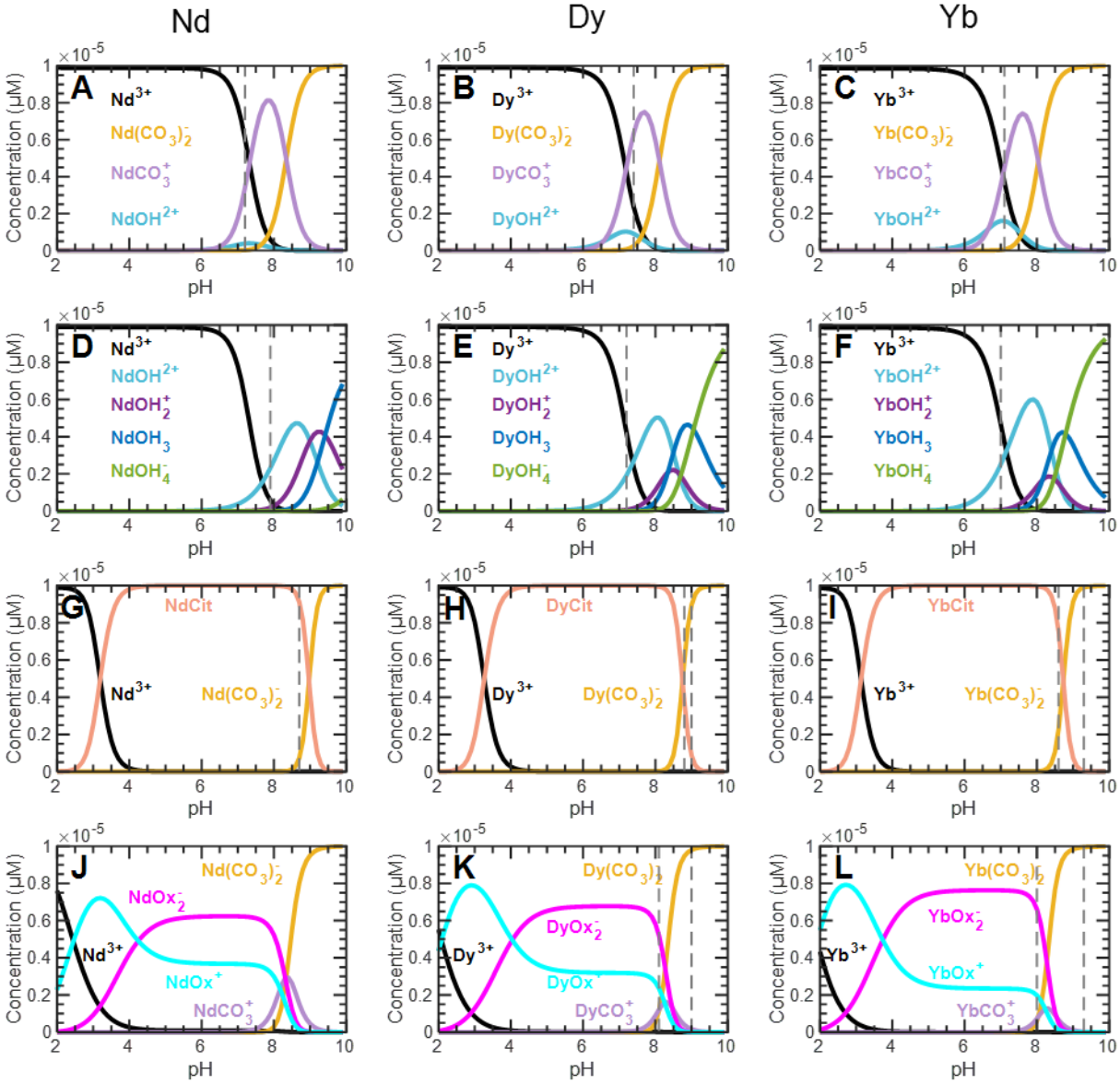

Figure S2. Speciation diagrams of rare earth elements. (A-C) DIC in equilibrium with atmospheric CO_2, (D-F) CO_2-free conditions, (G-I) DIC in equilibrium with atmospheric CO_2 in the presence of 100 μM citric acid, (J-L) DIC in equilibrium with atmospheric CO_2 in the presence of 100 μM oxalic acid. The electrolyte was 10 mM NaCl, the total REE concentration was 10 μM, and atmospheric $\log P_{CO2}$ was assumed to be -3.42. The dashed line indicates the pH value at which REE precipitates based on solubility calculations. In (J), a dashed line is not shown because Nd is predicted to precipitate at all pH values (2-10) indicated in the figure.

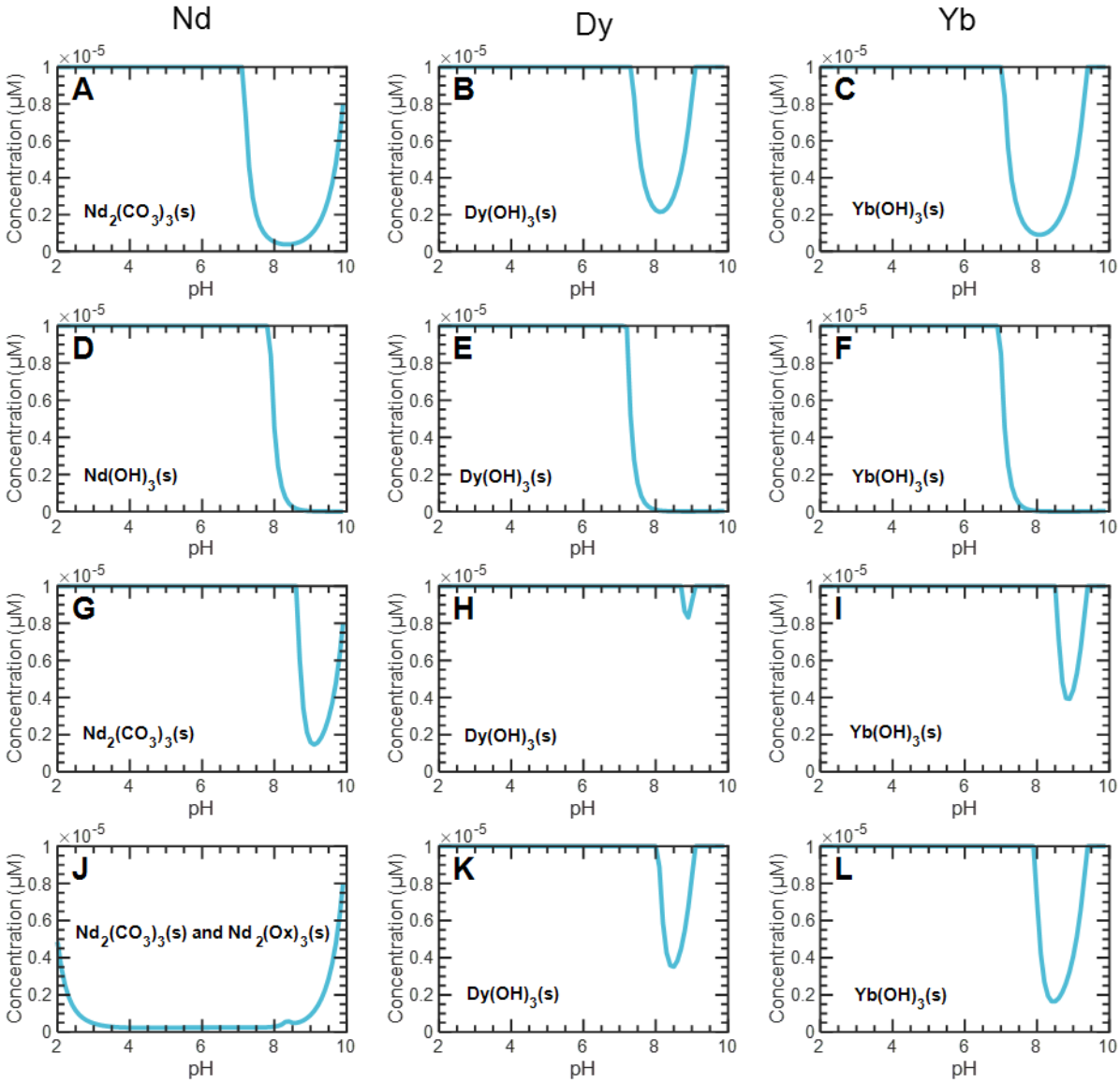

Figure S3. Total dissolved REE concentrations in equilibrium with the solubility-controlling solid phase (in annotation). (A-C) DIC in equilibrium with atmospheric CO_2, (D-F) CO_2-free conditions, (G-I) DIC in equilibrium with atmospheric CO_2 in the presence of 100 μM citric acid, (J-L) DIC in equilibrium with atmospheric CO_2 in the presence of 100 μM oxalic acid. The electrolyte was 10 mM NaCl, the total REE concentration was 10 μM, and atmospheric $\log P_{CO2}$ was assumed to be -3.42.

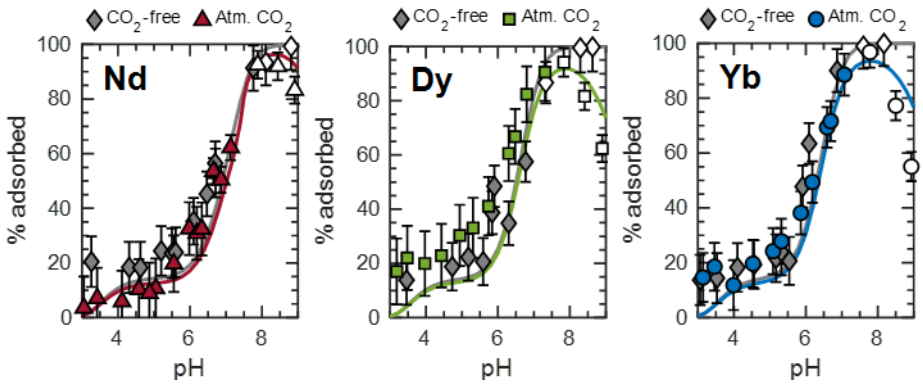

Figure S4. The effect of pH and DIC in equilibrium with atmospheric CO_2 on the retention of REEs (10 µM) to kaolinite (0.2 g/L) in the presence of 10 mM NaCl. Markers represent experimental data; open white markers show data points at which solubility calculations indicate the possibility of REE precipitation. Solid lines represent the output from the SCM.

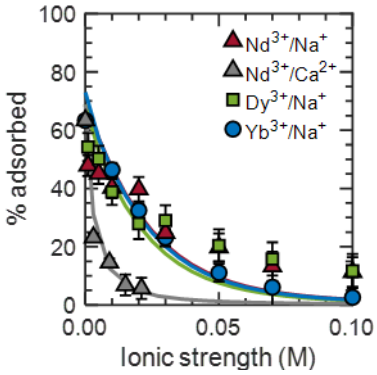

Figure S5. The effect of electrolyte type (NaCl and $CaCl_2$) and concentration on adsorption of REEs (1 µM) to kaolinite at pH 4. The solutions in all experiments were in equilibrium with atmospheric CO_2. Markers represent experimental data; solid lines represent the output from the SCM.

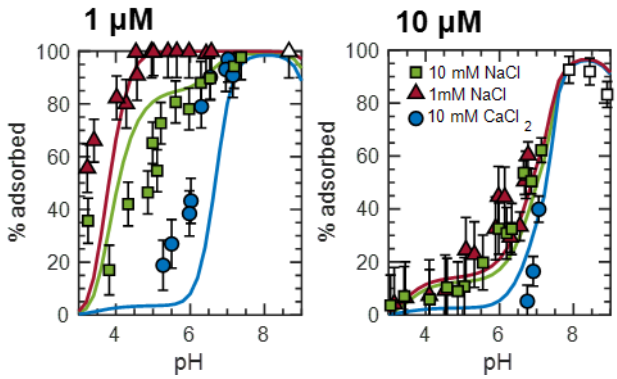

Figure S6. The effect of electrolyte type and concentration on Nd retention to kaolinite (0.2 g/L). Total Nd concentration was 1 µM and 10 µM. The solutions in all experiments were in equilibrium with atmospheric CO_2. Markers represent experimental data; solid lines represent the output from the surface complexation model. Open white markers show data points at which solubility calculations indicate the possibility of REE precipitation.

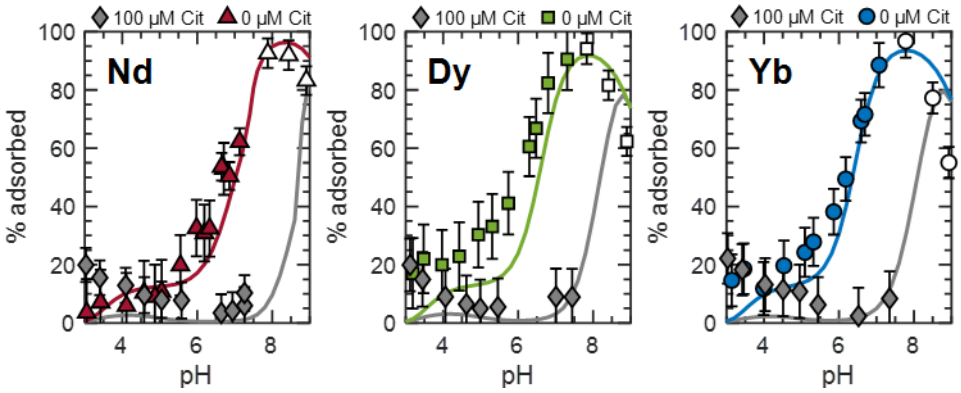

Figure S7. The effect of citric acid (100 µM) on retention of REEs (10 µM) to kaolinite in the presence of 10 mM NaCl. The solutions in all experiments were in equilibrium with atmospheric CO_2. Markers represent experimental data; open white markers show data points at which solubility calculations indicate the possibility of REE precipitation. Solid lines represent the output from the SCM with ternary surface complexes (REE-citric acid-kaolinite).

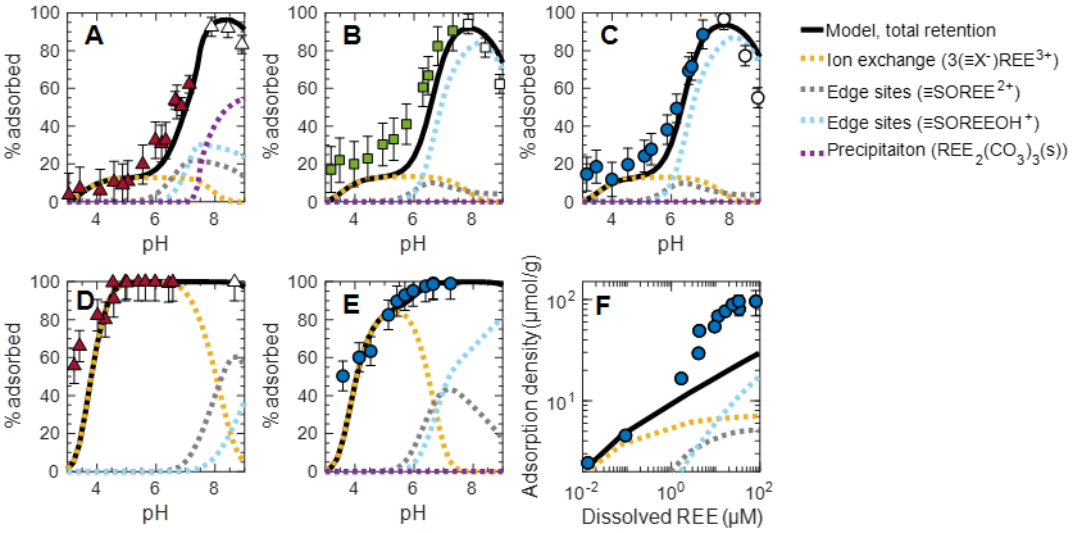

Figure S8. Detailed overview of the surface complexation model output (lines) for selected experiments. Markers represent retention of (A) 10 µM Nd, (B) 10 µM Dy, (C) 10 µM Yb, (D) 1 µM Nd, (E) 1 µM Yb, (F) 0.1-100 µM Yb to kaolinite (0.2 g/L). DIC in all experiments was in equilibrium with atmospheric CO_2. The electrolyte was 10 mM NaCl in all panels, except (D), where NaCl concentration was 1 mM. Open white markers show data points at which solubility calculations indicate the possibility of REE precipitation.

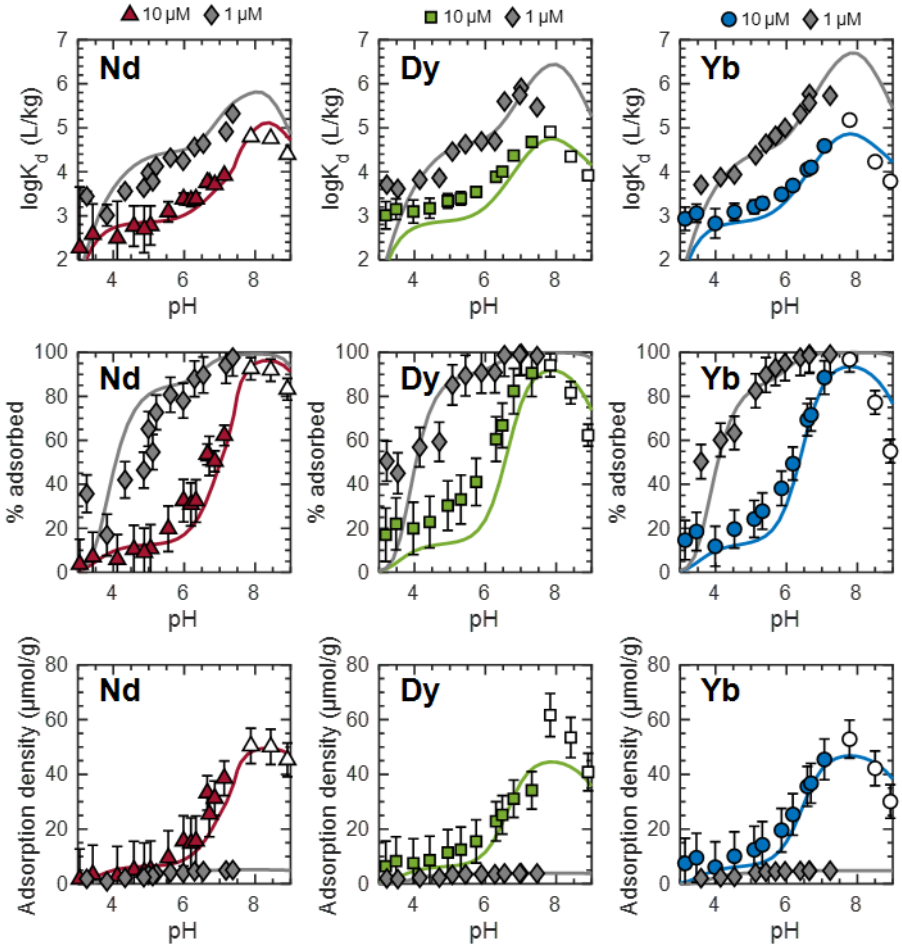

Figure S9. The effect of the total REE concentration (1 µM or 10 µM) on REE retention to kaolinite (0.2 g/L) in the presence of 10 mM NaCl. The solutions in all experiments were in equilibrium with atmospheric CO_2. Markers represent experimental data; open white markers show data points at which solubility calculations indicate the possibility of REE precipitation. Solid lines represent the output from the SCM. The top row shows logK_d values, the middle row shows %adsorbed values, and the bottom row shows adsorption densities.

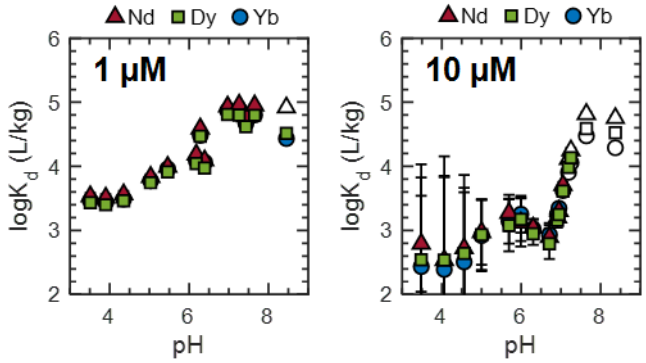

Figure S10. Retention of REEs in a mixed batch (1 µM or 10 µM of each REE) in the presence of 10 mM NaCl. The solutions in all experiments were in equilibrium with atmospheric CO_2. Markers represent experimental data; open white markers show data points at which solubility calculations indicate the possibility of REE precipitation.

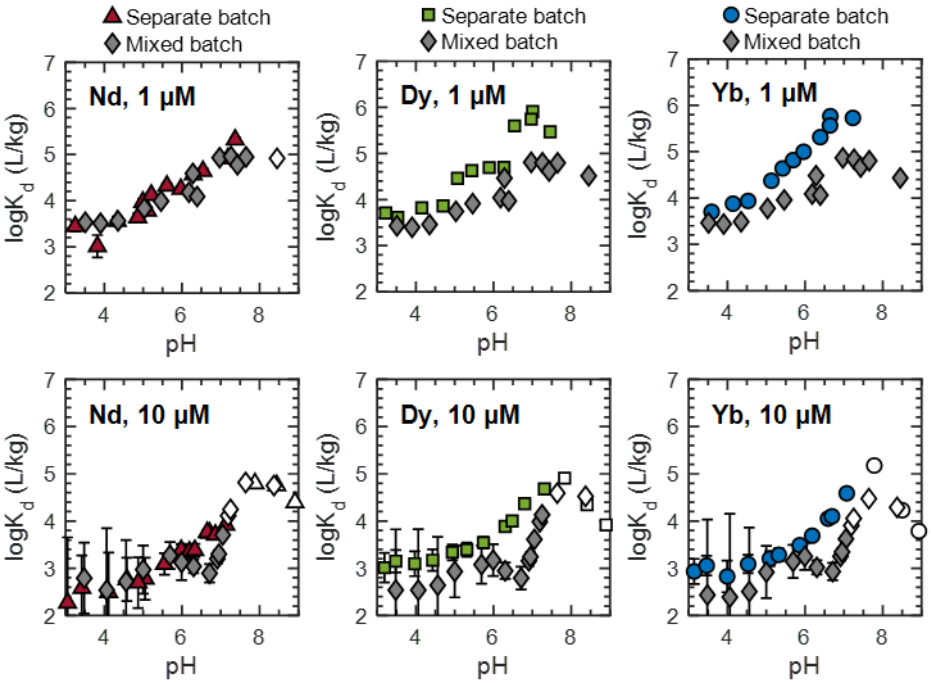

Figure S11. Retention of REEs in mixed batch and separate batches (1 µM or 10 µM of each REE) in the presence of 10 mM NaCl. The solutions in all experiments were in equilibrium with atmospheric CO_2. Markers represent experimental data; open white markers show data points at which solubility calculations indicate the possibility of REE precipitation.

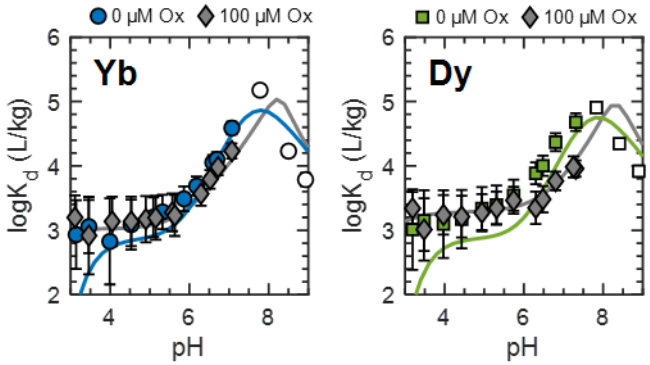

Figure S12. The effect of oxalic acid (100 µM) on retention of Dy and Yb (10 µM) to kaolinite in the presence of 10 mM NaCl. The solutions in all experiments were in equilibrium with atmospheric CO_2. Markers represent experimental data; open white markers show data points at which solubility calculations indicate the possibility of REE precipitation. Solid lines represent the output from the SCM with ternary surface complexes (REE-oxalic acid acid-kaolinite). The effect of oxalic acid on Nd was not investigated due to the propensity of Nd to precipitate with oxalic acid.

Table S2. Structural model fitting results for the EXAFS spectra of Yb adsorbed to kaolinite.

Sample	Path	CN	R (Å)	σ^2 (Å^2)	ΔE_0 (eV)	S_0^2	R-factor	V/NIDP	χ_v^2	R range (Å)	k range (Å^{-1})
10 μM Yb, 200 mg/L kaolinite, 100 μM citrate, 10 mM NaCl, pH 3.5	Yb-O_1	5.4±0.7	2.307±0.008	0.001±0.001	10±1	1.0	0.011	6/13.7	0.78	1.5-3.5	3.0-13.0
	Yb-O_2	2.5±0.3	2.455±0.018[a]	0.001±0.001							
10 μM Yb, 200 mg/L kaolinite, 10 mM NaCl, pH 3.5	Yb-O_1	5.7±1.0	2.327±0.011	0.002±0.001	11±1	1.0	0.019	6/13.7	1.60	1.5-3.5	3.0-13.0
	Yb-O_2	2.2±0.5	2.483±0.029	0.002±0.001							
10 μM Yb, 200 mg/L kaolinite, 1 mM NaCl, pH 4	Yb-O_1	4.9±0.7	2.314±0.009	0.001±0.001	11±1	1.0	0.016	6/13.7	0.91	1.5-3.5	3.0-13.0
	Yb-O_2	2.7±0.3	2.459±0.017	0.001±0.001							
10 μM Yb, 200 mg/L kaolinite, 10 mM NaCl, pH 6	Yb-O_1	7.8±1.5	2.349±0.014	0.007±0.002	11±2	1.0	0.038	6/13.7	1.61	1.5-3.5	3.0-13.0
	Yb-O_2	1.5±1.4	2.576±0.060	0.007±0.002							
10 μM Yb, 200 mg/L kaolinite, 10 mM NaCl, pH 7	Yb-O_1	5.4±1.5	2.289±0.021	0.006±0.002	8±1	1.0	0.006	6/12.5	0.32	1.5-3.5	3.0-12.0
	Yb-O_2	2.7±0.9	2.421±0.033	0.006±0.002							
10 μM Yb, 200 mg/L kaolinite, 100 μM citrate, 10 mM NaCl, pH 7	Yb-O_1	5.8±1.6	2.326±0.019	0.005±0.002	11±2	1.0	0.024	6/12.5	1.24	1.5-3.5	3.0-12.0
	Yb-O_2	1.9±0.7	2.497±0.058	0.005±0.002							

[a]The σ^2 value for the two Yb-O paths were constrained to be equal.

Fitting parameter: coordination numbers (CN); interatomic distance (R); Debye-Waller factor (σ^2); difference in the threshold Fermi level between data and theory (ΔE_0); amplitude reduction factor (S_0^2); reduced χ squared value (χ_v^2) and R-factor are goodness-of-fit parameters;[12] V is the number of variables; NIDP is the number of independent points.

Development of the diffuse double layer model (DLM) surface complexation model.

The surface complexation model (SCM) was developed based on two mechanisms: ion exchange and surface complexation to edge sites. We interpreted surface complexation to edge sites using the diffuse double-layer model.

The first step was developing the ion exchange model based on the calculated CEC (22.5 meq/kg) by optimizing for Gaines-Thomas coefficients (K_{GT}). Ion exchange reactions dominate at low pH ranges; therefore, we used data with pH < 4.5 in the fitting to prevent adsorption reactions on edge sites from affecting the determination of the Gaines-Thomas coefficients. The combination of four coefficients ($K_{GT,Nd/H}$, $K_{GT,Dy/H}$, $K_{GT,Yb/H}$, $K_{GT,Na/H}$) that resulted in the least residual sum of squares (RSS) is listed in Table 1. Adsorption data with $CaCl_2$ as an electrolyte and pH < 5 were fitted separately to find $K_{GT,Ca/H}$. The fitted Gaines-Thomas coefficients for Na^+/H^+ and Ca^{2+}/H^+ exchange agree well with published literature.[13]

The second step was choosing constraints on edge site density. Studies that calculated site density using crystallographic calculations report site densities in the range of 7.6-8.2 nm^{-2} based on the area of edge sites.[14,15] Most studies report site density based on BET surface area, and only a few studies measured a proportion of the area of edges to the BET surface area and reported a wide range of values (8-40% of BET surface area).[16–18] We assumed that edge sites comprise 40% of the total BET area to obtain the maximum adsorption capacity similar to the one observed in the isotherm experiment (19-23 μM) (Eq. S5). The total site density used in the SCM is 3.3 nm^{-2} BET surface area (21.5 m^2/g) or 8.2 nm^{-2} edge surface area (assuming that edges make up 40% of the BET surface area).

$$8.2\,\frac{\text{sites}}{\text{nm}^2\text{edge}} * \frac{\text{mol}}{6.023\times10^{23}\ \text{sites}} * 0.4\,\frac{\text{m}^2\ \text{edge}}{\text{m}^2\ \text{BET}} * 10^{18}\,\frac{\text{nm}^2\text{BET}}{\text{m}^2\text{BET}} * 21.5\,\frac{\text{m}^2\text{BET}}{\text{g}} * 0.2\,\frac{\text{g}}{\text{L}} = 23.4\ \mu\text{M}$$

(Eq. S5)

The third step was fitting a titration curve of the kaolinite suspension by varying the deprotonation constant ($\equiv SOH \rightleftharpoons \equiv SO^- + H^+$) while keeping Na^+/H^+ ion exchange reaction from the first step (Figure S13). We assumed only one site to characterize edge sites (≡S) because the titration fit was satisfactory ($R^2 = 0.95$). Using a single site type oversimplifies the kaolinite structure containing different surfaces (aluminol basal plane, silanol basal plane, aluminol edge sites, and silanol edge sites), but macroscopic adsorption experiments alone cannot provide sufficient information to differentiate between aluminol vs. silanol sites or a particular crystallographic plane the adsorption sites are on. The fitting of another deprotonation constant ($\equiv SOH_2 \rightleftharpoons \equiv SOH + H^+$) was not required because the ion exchange reaction between Na^+ and H^+ ions ($\log K_{GT,Na/H} = -2.3$) could adequately explain the titration curve at low pH values (< 5). A combination of the Gaines-Thomas coefficient ($K_{GT,Na/H}$) and the optimized deprotonation constant was sufficient to reproduce the titration fitting accurately enough to capture the main deprotonation trends with the minimum number of model parameters. Titration data and the accompanying fits agree well with other studies reporting titration of kaolinite suspensions (Figure S13).

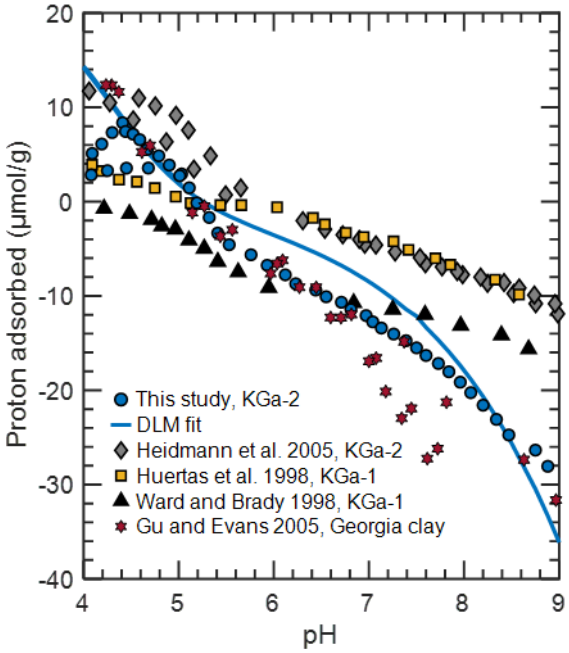

Figure S13. Proton adsorption to kaolinite as a function of pH in CO_2-free conditions. Kaolinite loading was 5 g/L in this study. All studies used 10 mM electrolyte concentration (NaCl in this study and Ward and Brady[19], $KClO_4$ in Huertas et al.[20], and $NaNO_3$ in Heidmann et al.[21] and Gu and Evans[22]).

The fourth step was to determine the stoichiometry of surface complexes and the associated equilibrium constants that provided the best fit of the model to the experimental data. We assumed two surface complexes ($\equiv SOREE^{2+}$ and $\equiv SOREEOH^{+}$) representing the simplest stoichiometry for each REE. We excluded data points featuring water chemistry conditions that favor precipitation (mostly pH > 7) and excluded precipitation reactions from the fitting. Equilibrium constants (logK values) for each REE were fitted separately and to the nearest 0.1 units. The intrinsic equilibrium constants providing the best fit were those with the minimum RSS, and the success criterion was $R^2 > 0.9$. Competitive adsorption data were not included in the model optimization, but they were instead used for checking the model's performance for predicting adsorption at conditions not included in the optimization.

The model optimization included a sensitivity analysis to understand the uncertainty of the equilibrium constant. After finding the equilibrium constant that provided the minimum residual sum of squares (RSS), we varied it to determine how high or low it could be while maintaining the RSS within 5% of the minimum RSS. The resulting range of equilibrium constants provides uncertainty estimates for the optimal value of the constant.

The fifth step was fitting experiments with organic ligands (citric acid and oxalic acid). Organic ligands can potentially affect REE adsorption to kaolinite by (1) forming an aqueous complex (Figures S3G-S3L), and (2) adsorbing to kaolinite separately from REEs and thereby occupying adsorption sites, and (3) forming ternary surface complexes (REE-organic ligand-kaolinite). The simplest way to model adsorption with organic ligands is to assume a system in which organic ligands and REEs adsorb to kaolinite independently of one another without ternary complexation. Ternary surface complexes can be added if the model fit with the simple system is unsatisfactory.

The adsorption of organic ligands to kaolinite (without REEs) has been studied previously with surface complexation modeling.[19,23] We could not use these models directly because both of the previous studies assumed different surface complexation models from the one we used (Table S3). We re-optimized equilibrium constants for the binding of organic ligands to kaolinite based on the adsorption data from these previous studies with DLM (Table 1 and Figure S14). Although the previous studies used different sources of kaolinite, we assumed that the site density from this study (8.2 nm^{-2} based on edge surface area) applies to the kaolinite that they used. We re-calculated site concentration based on the BET surface area of kaolinite and kaolinite loading used in those studies (Table S3).

Table S3. Differences between this study and the published literature describing the adsorption of organic ligands to kaolinite.

	This study	Lackovic et al.[23]	Ward and Brady[19]
Organic ligand	Both citrate and oxalate	Citrate	Oxalate
Type of kaolinite	KGa-2	Commercial	KGa-1
Electrolyte	10 mM NaCl	10 mM $KCiO_4$	10 mM NaCl
Mineral loading	0.2 g/L	6.8 g/L	100 g/L
BET surface area	21.5 m^2/g	14.7 m^2/g	8.6 m^2/g
Model type	Double layer	Extended constant capacitance	Triple layer

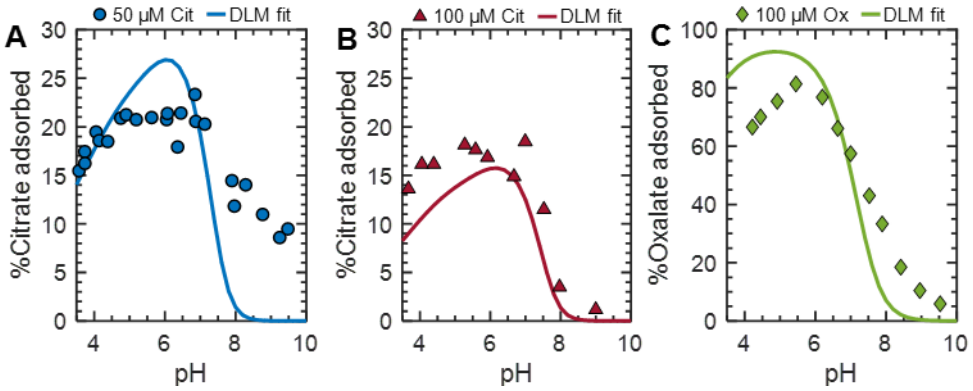

Figure S14. Adsorption of (A) 50 µM citrate, (B) 100 µM citrate, and (C) 100 µM oxalate to kaolinite. Markers represent experimental data from the published literature;[19,23] solid lines represent the output from the surface complexation model.

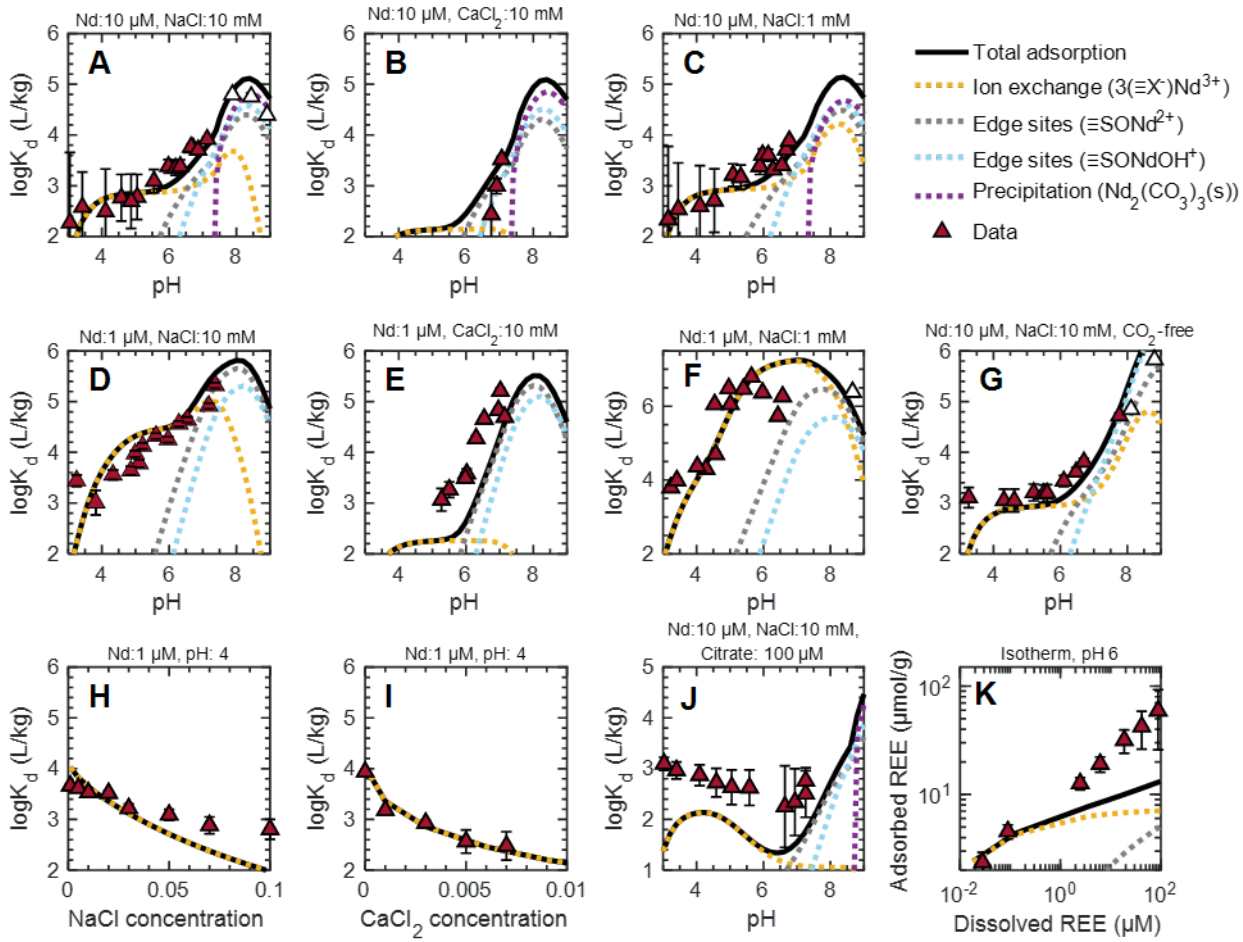

Figure S15. Detailed overview of the DLM-based surface complexation model output (lines) in all experiments with Nd. Markers represent experimental data; open white markers show data points at which solubility calculations indicate the possibility of REE precipitation. DIC in all experiments was in equilibrium with atmospheric CO_2 (except panel G, which corresponds to the CO_2-free experiment).

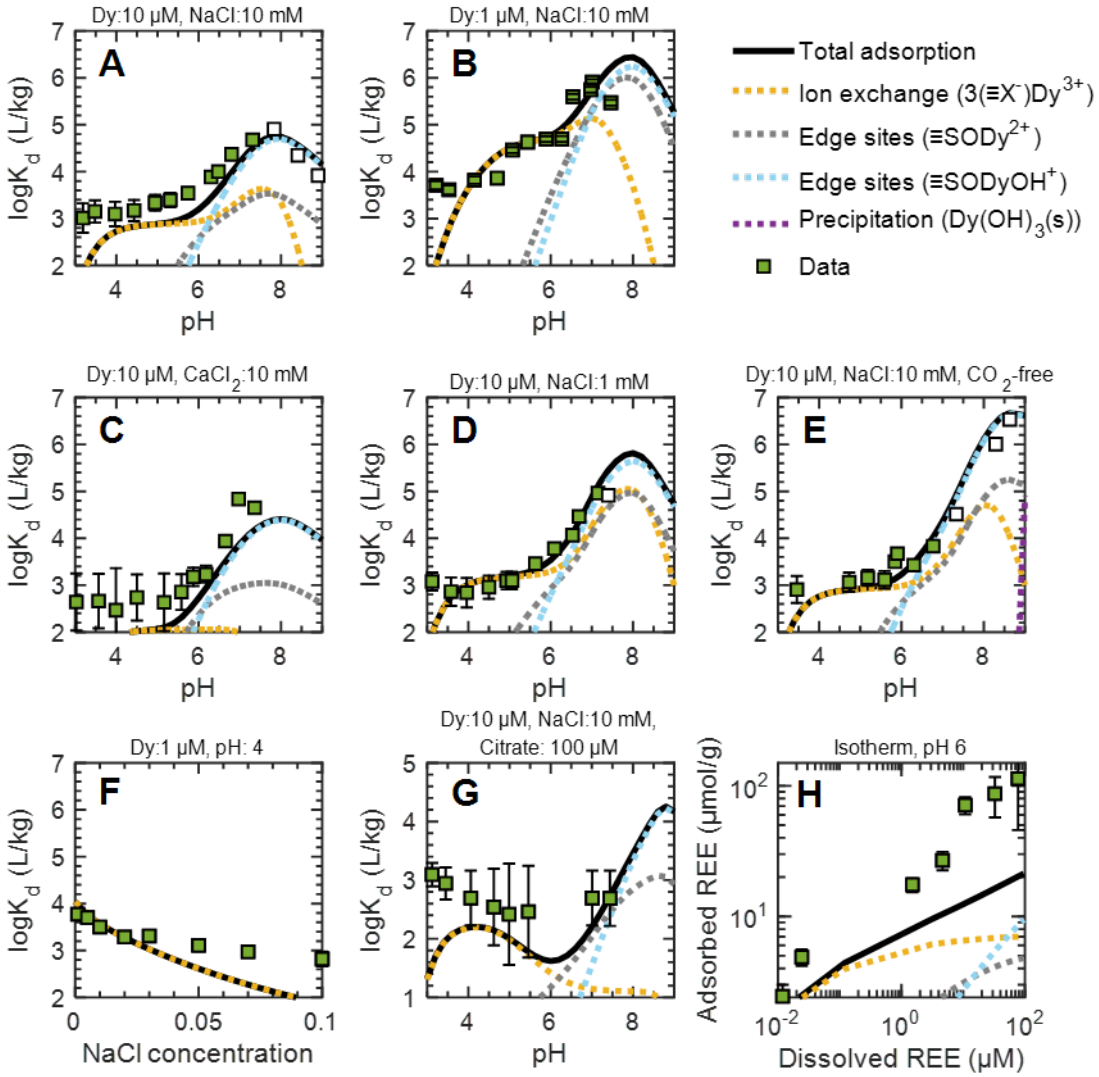

Figure S16. Detailed overview of the DLM-based surface complexation model output (lines) in all experiments with Dy. Markers represent experimental data; open white markers show data points at which solubility calculations indicate the possibility of REE precipitation. DIC in all experiments was in equilibrium with atmospheric CO_2 (except panel E, which corresponds to the CO_2-free experiment).

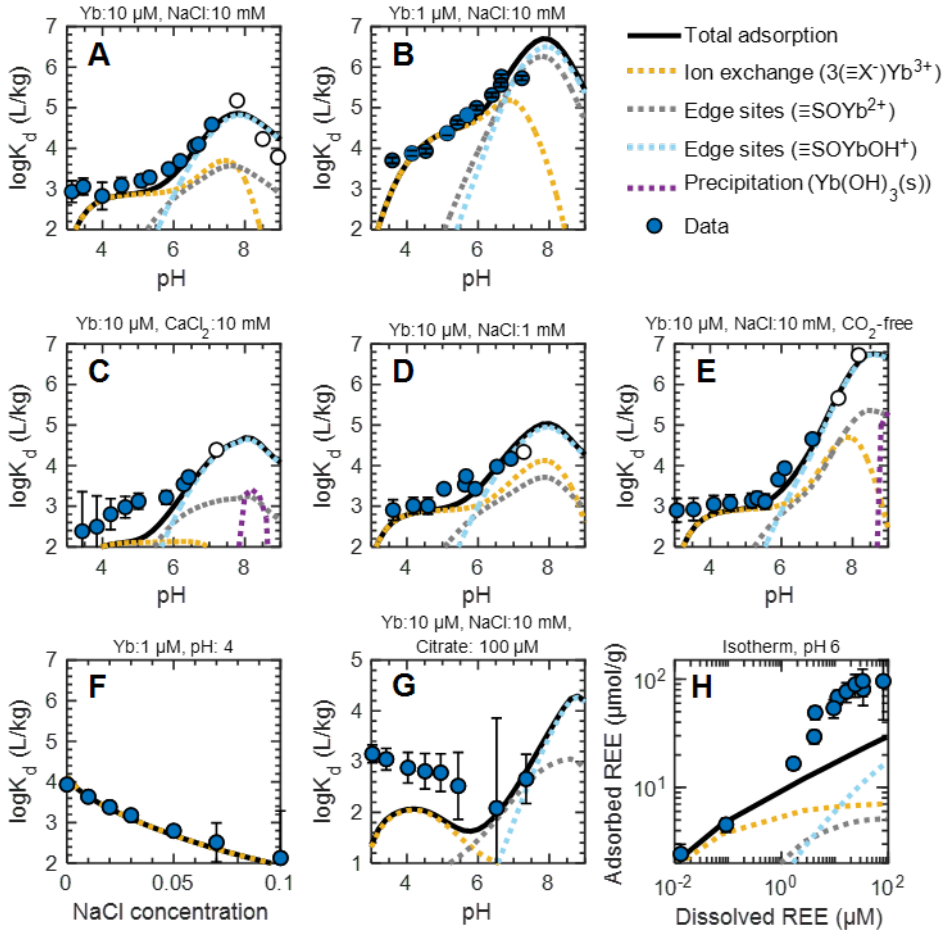

Figure S17. Detailed overview of the DLM-based surface complexation model output (lines) in all experiments with Yb. Markers represent experimental data; open white markers show data points at which solubility calculations indicate the possibility of REE precipitation. DIC in all experiments was in equilibrium with atmospheric CO_2 (except panel E, which corresponds to the CO_2-free experiment).

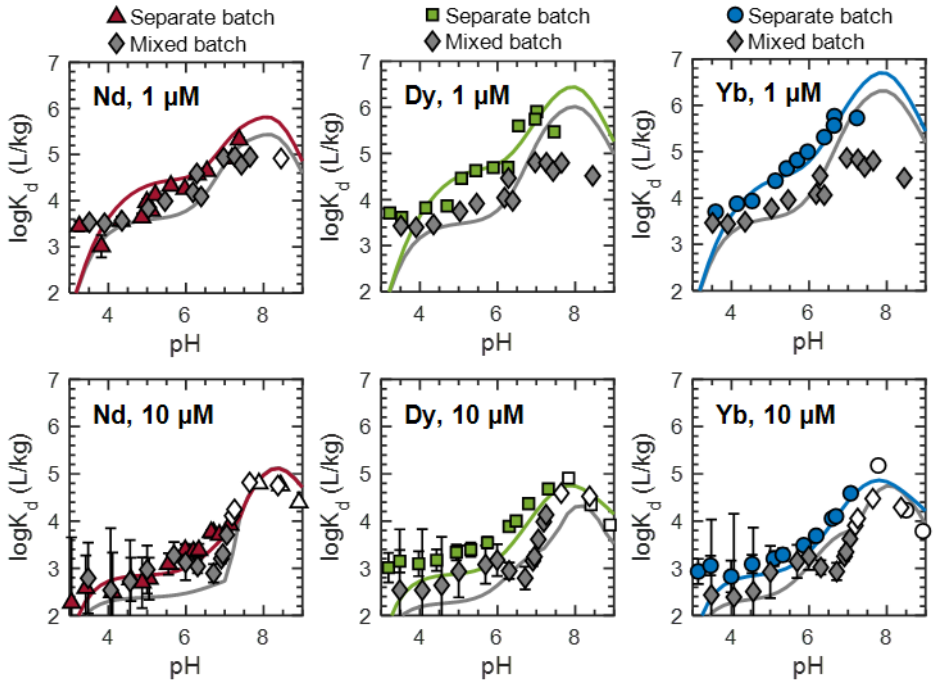

Figure S18. Comparison of REE retention in separate batches (Nd or Dy or Yb, colored markers) and mixed batches (Nd and Dy and Yb, grey diamond markers) in the presence of 10 mM NaCl and 0.2 g/L kaolinite. The solutions in all experiments were in equilibrium with atmospheric CO_2. Markers represent experimental data; open white markers show data points at which solubility calculations indicate the possibility of REE precipitation. Solid lines represent the output from the surface complexation model.

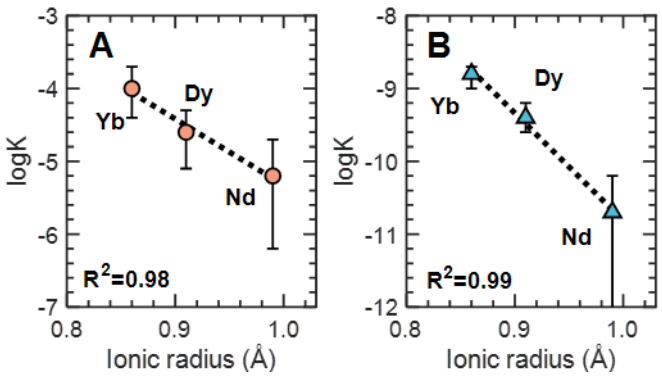

Figure S19. Equilibrium constants for adsorption reactions on edge sites in DLM for (A) $\equiv SOREE^{2+}$ and (B) $\equiv SOREEOH^{+}$ surface complexes. Ionic radii were taken from Moldoveanu and Papangelakis.[24] Markers represent the fitted equilibrium constants, whereas lines represent the linear function fitting. Error bars represent a range of equilibrium constants, which result in RSS within 5% of the minimum RSS.

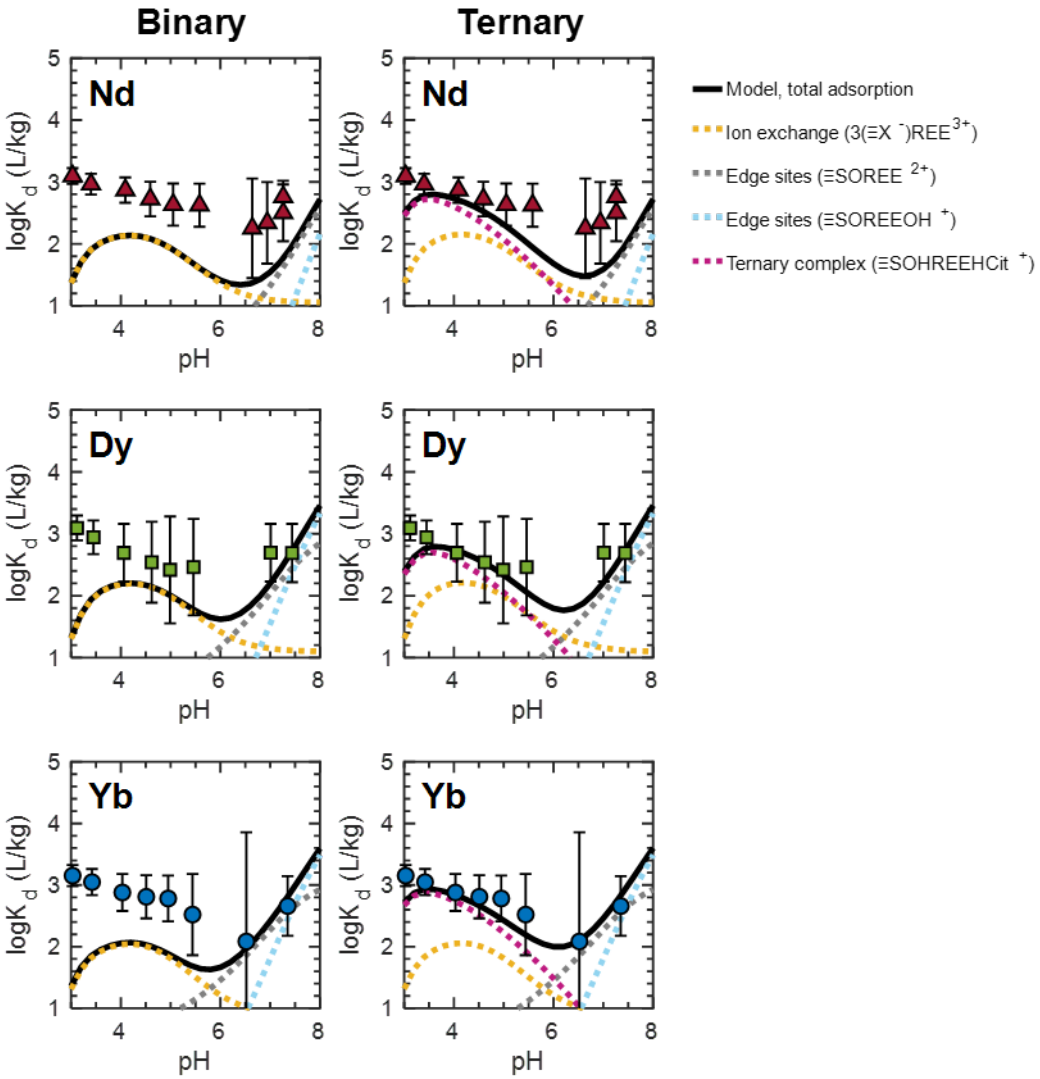

Figure S20. Modeling the adsorption of 10 μM REE to kaolinite (0.2 g/L) in the presence of citric acid (100 μM) with only binary citrate-kaolinite and REE-kaolinite surface complexation reactions (left column) and with the inclusion of a ternary citrate-REE-kaolinite surface complex (right column). Optimized constants are listed in Table S4. The solutions in all experiments contained 10 mM NaCl as the electrolyte and were in equilibrium with atmospheric CO_2. Markers represent experimental data; lines represent the output from the SCM.

Table S4. Equilibrium constants (DLM) for REE-citric acid-kaolinite ternary surface complexes[a].

Surface reactions	logK[b]
$\equiv SOH + Nd^{3+} + Cit^{3-} + H^+ \rightleftharpoons \equiv SOHNdHCit^+$	15.2
$\equiv SOH + Dy^{3+} + Cit^{3-} + H^+ \rightleftharpoons \equiv SOHDyHCit^+$	15.0
$\equiv SOH + Yb^{3+} + Cit^{3-} + H^+ \rightleftharpoons \equiv SOHYbHCit^+$	15.5

[a]This table is complementary to Tables 1 and 2 in the main text.

[b]Activity of a surface complex in intrinsic equilibrium constants describing complexation to edge sites is expressed as a mole fraction. The site density of edge sites (≡S) was assumed to be 8.2 nm^{-2} based on edge surface area (assuming that edge sites make up 40% of BET surface area or 8.6 m^2/g).

Adsorption of REEs to kaolinite in the presence of oxalic acid

Oxalic acid does not affect the adsorption of Yb at any of the pH values studied, but it does slightly decrease the adsorption of Dy at pH > 6 (Figure S12). The solubility diagram for Nd in the presence of oxalic acid (Figure S3J) predicts precipitation of Nd-oxalate solid at the given water chemistry conditions (100 µM oxalic acid, pH 3-9, and 10 µM Nd); therefore, the effect of oxalic acid on Nd adsorption was not examined in this study. REE-oxalic acid aqueous complexes ($REEOx^+$ and $REEOx_2^-$) are dominant at pH 3-9 and are expected to decrease adsorption in the presence of oxalic acid (Figure S2). However, the little to no effect from oxalic acid on the adsorption of Dy and Yb suggests that ternary surface complexes are formed (REE-oxalic acid-kaolinite). This observation agrees with the SCM because the SCM fails to predict the data accurately with the binary system assumption. Two ternary surface complexes are required to capture adsorption trends at pH > 5.5 (≡SOREEOx) and pH < 5.5 (≡SOHREEOx$^+$) (Figure S21 and Table S5).

The equilibrium constants of these ternary complexes were optimized based on stability constants from Schijf and Byrne.[10] There is a wide range of stability constants for REE-oxalate aqueous complexes reported in the published literature, especially for Yb (Table S6). We tried to improve the fit of the model with just binary reactions to the data by varying the stability constants, but the SCM still underestimates adsorption (Figure S22).

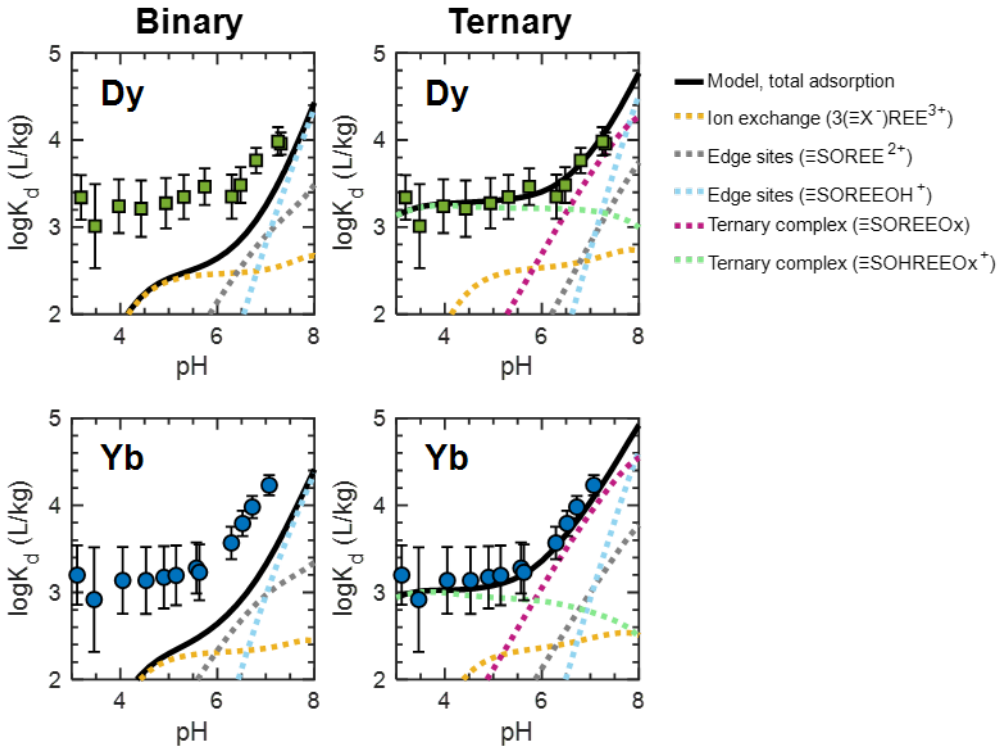

Figure S21. Modeling the adsorption of 10 µM REE to kaolinite (0.2 g/L) in the presence of oxalic acid (100 µM) with only binary oxalate-kaolinite and REE-kaolinite surface complexation reactions (left column) and with the inclusion of a ternary oxalate-REE-kaolinite surface complex (right column). The solutions in all experiments contained 10 mM NaCl as the electrolyte and were in equilibrium with atmospheric CO_2. Markers represent experimental data; lines represent the output from the SCM.

Table S5. Equilibrium constants (DLM) for REE-oxalic acid-kaolinite ternary surface complexes[a].

Reaction	logK[b]
$\equiv SOH + Dy^{3+} + Ox^{2-} \rightleftharpoons \equiv SOHDyOx^{+}$	9.3
$\equiv SOH + Yb^{3+} + Ox^{2-} \rightleftharpoons \equiv SOHYbOx^{+}$	9.3
$\equiv SOH + Dy^{3+} + Ox^{2-} \rightleftharpoons \equiv SODyOx + H^{+}$	5.0
$\equiv SOH + Yb^{3+} + Ox^{2-} \rightleftharpoons \equiv SOYbOx + H^{+}$	5.7

[a]This table is complementary to Tables 1 and 2 in the main text.

[b]Activity of a surface complex in intrinsic equilibrium constants describing complexation to edge sites is expressed as a mole fraction. The site density of kaolinite edge sites (≡S) was assumed to be 8.2 nm^{-2} based on edge surface area (assuming that edge sites make up 40% of BET surface area or 8.6 m^2/g).

Table S6. Literature review of stability constants for Yb-oxalate aqueous complexes.

Reference	$YbOx^{+}$	$YbOx_2^{-}$	$YbOx_3^{3-}$
[10]	6.95	11.75	
[4]	6.74	11.44	
[25]	7.82	12.28	14.77
[26]	7.02	11.95	
[9]	7.30	11.89	

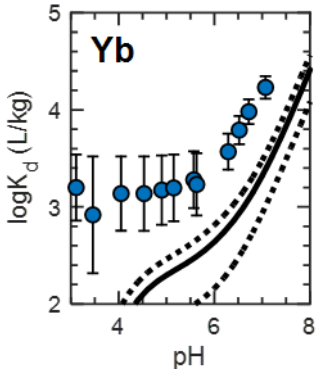

Figure S22. Modeling the adsorption of 10 μM Yb to kaolinite (0.2 g/L) in the presence of oxalic acid (100 μM) with the binary system. The solutions in all experiments contained 10 mM NaCl as the electrolyte and were in equilibrium with atmospheric CO_2. Markers represent experimental data. Solid lines show the output from the SCM, and dotted lines show how this output changes depending on the choice of stability constant. The upper dashed line is based on stability constants from NIST,[4] the lower dashed line is based on Gammons and Wood,[25] and the solid gray line is based on Schijf and Byrne.[10]

Non-electrostatic model (NEM)

A non-electrostatic model (NEM) was developed in addition to the DLM to assess the effect of the electrostatic interactions on model predictions of the experimental data (Table S7). The NEM included the same set of Gaines-Thomas coefficients for ion exchange as DLM (Table 1). Unlike the DLM, The NEM required two sites to fit titration data (Figure S24). The NEM titration fit was unsatisfactory with one site type (≡S), requiring the addition of another site type (≡Y). To obtain an accurate model output for the titration curve, the ≡Y sites must have a smaller site concentration (2.3 μM) and a lower pK_a than ≡S sites (21.1 μM). The total site concentration (≡Y and ≡S) was fixed at 23.4 μM based on the maximum observed adsorption capacity from isotherm experiments (Eq. S5). The ≡S sites do not deprotonate over the studied pH range. These two types of sites do not provide any information beyond the affinity towards proton ions captured by titration curves. The maximum adsorption capacity of 113 μmol/g (23 μM) observed in isotherm experiments suggests that the ≡S sites are responsible for most of the observed REE adsorption. The adsorption associated with the second type of sites (≡Y) cannot exceed the small ≡Y site concentration (2.3 μM). Therefore, REE adsorption was assumed to happen on ≡S sites only to check NEM's fit of data from isotherm experiments.

Overall, the NEM equilibrium constants increase as REEs become heavier, similar to the trend in equilibrium constants in the DLM but without the strong correlation observed in Figure 7. In the NEM, only one surface complex was sufficient to describe Nd adsorption. The NEM predicted adsorption in isotherm experiments very accurately, suggesting the electrostatic term in the DLM affects its performance at high REE concentrations. The NEM captured the main trends of adsorption, but when predicting adsorption as a function of pH, it underestimates adsorption at low REE concentrations (Figure S23). The NEM also required an additional level of complexity (two sites) compared to the DLM.

Table S7. NEM equilibrium constants describing adsorption to edge sites[a].

Reaction	logK[b]
Deprotonation of edge sites (logK)[b]	
$\equiv SOH \rightleftharpoons \equiv SO^- + H^+$	-9.8
$\equiv YOH \rightleftharpoons \equiv YO^- + H^+$	-6.2
Adsorption of REEs to edge sites (logK)[b]	
$\equiv SOH + Nd^{3+} \rightleftharpoons \equiv SONd^{2+} + H^+$	-1.3
$\equiv SOH + Dy^{3+} \rightleftharpoons \equiv SODy^{2+} + H^+$	-1.1
$\equiv SOH + Yb^{3+} \rightleftharpoons \equiv SOYb^{2+} + H^+$	-0.9
$\equiv SOH + Nd^{3+} + H_2O \rightleftharpoons \equiv SONdOH^+ + 2H^+$	
$\equiv SOH + Dy^{3+} + H_2O \rightleftharpoons \equiv SODyOH^+ + 2H^+$	-7.8
$\equiv SOH + Yb^{3+} + H_2O \rightleftharpoons \equiv SOYbOH^+ + 2H^+$	-7.6

[a]Ion exchange reactions in NEM are the same as in DLM (Table 1 in the main text). The total site density of kaolinite edge sites (≡S plus ≡Y) was assumed to be 8.2 nm^{-2} based on edge surface area (assuming that edge sites make up 40% of BET surface area or 8.6 m^2/g). [b]Activity of a surface complex in intrinsic equilibrium constants is expressed as a mole fraction.

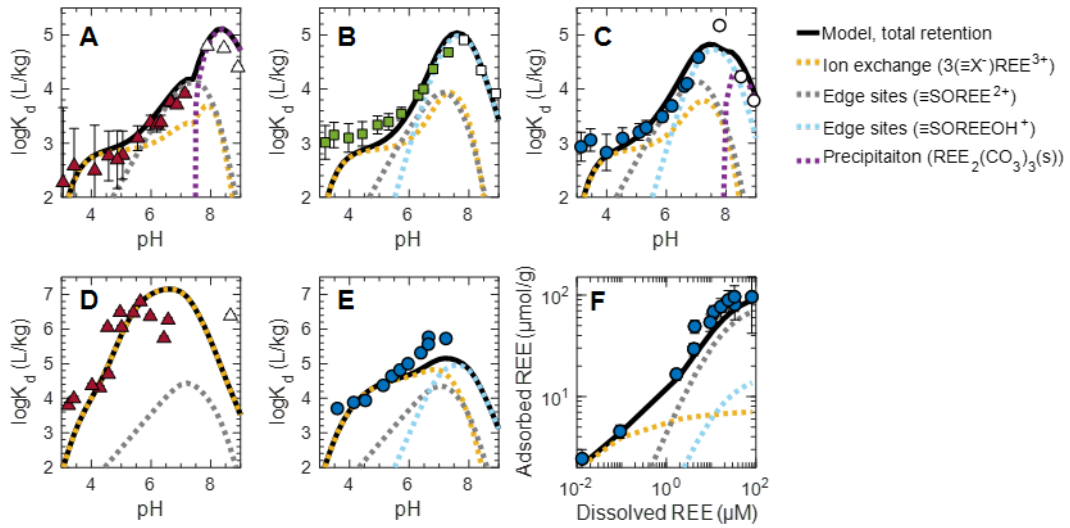

Figure S23. Detailed overview of the output of NEM (lines) in selected experiments. Markers represent retention of (A) 10 µM Nd, (B) 10 µM Dy, (C) 10 µM Yb, (D) 1 µM Nd, (E) 1 µM Yb, (F) 0.1-100 µM Yb to kaolinite (0.2 g/L). DIC in all experiments was in equilibrium with atmospheric CO_2. The electrolyte was 10 mM NaCl in all panels, except (D), where NaCl concentration was 1 mM. White markers show data points at which solubility calculations predict REE precipitation.

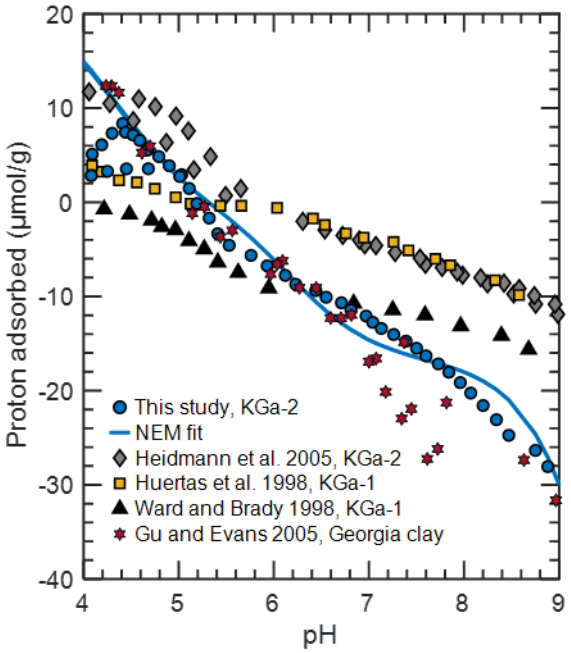

Figure S24. Proton adsorption to kaolinite as a function of pH in CO_2-free conditions. Kaolinite loading was 5 g/L in this study. All studies used 10 mM electrolyte concentration (NaCl in this study and Ward and Brady,[19] $KClO_4$ in Huertas et al.,[20] and $NaNO_3$ in Heidmann et al.,[21] and Gu and Evans[22]). The dotted line represents the output from NEM.

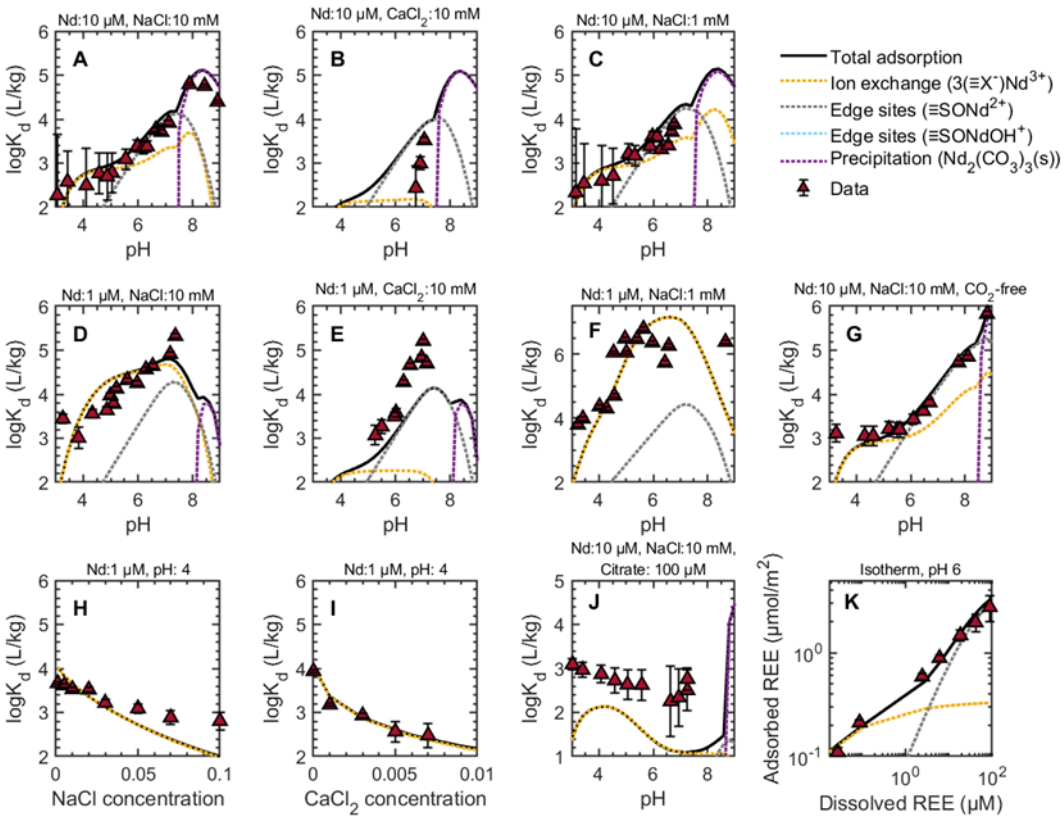

Figure S25. Detailed overview of the NEM-based surface complexation model output (lines) in all experiments with Nd. Markers represent experimental data; open white markers show data points at which solubility calculations indicate the possibility of REE precipitation. DIC in all experiments was in equilibrium with atmospheric CO_2 (except panel E, which corresponds to the CO_2-free experiment).

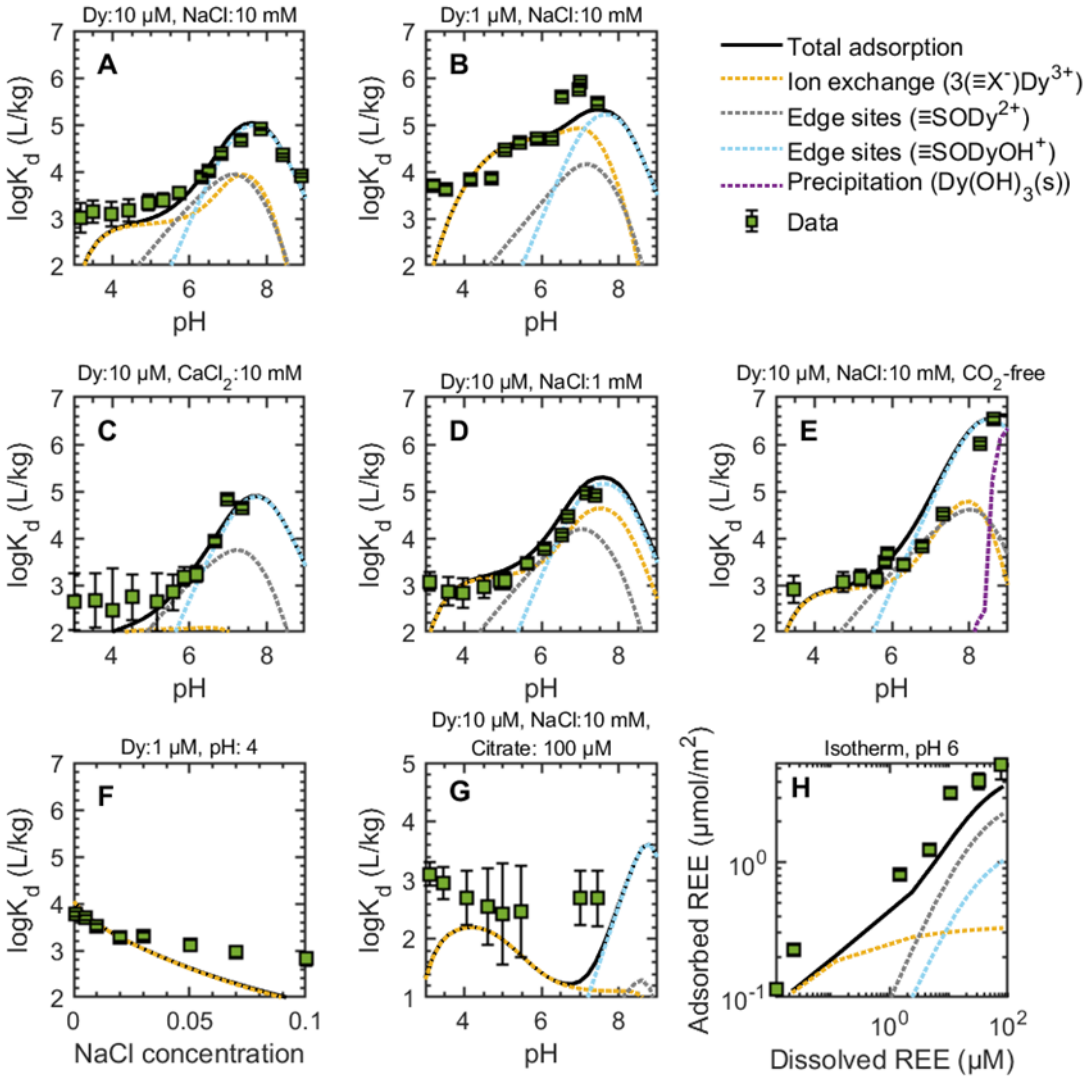

Figure S26. Detailed overview of the NEM-based surface complexation model output (lines) in all experiments with Dy. Markers represent experimental data; open white markers show data points at which solubility calculations indicate the possibility of REE precipitation. DIC in all experiments was in equilibrium with atmospheric CO_2 (except panel E, which corresponds to the CO_2-free experiment).

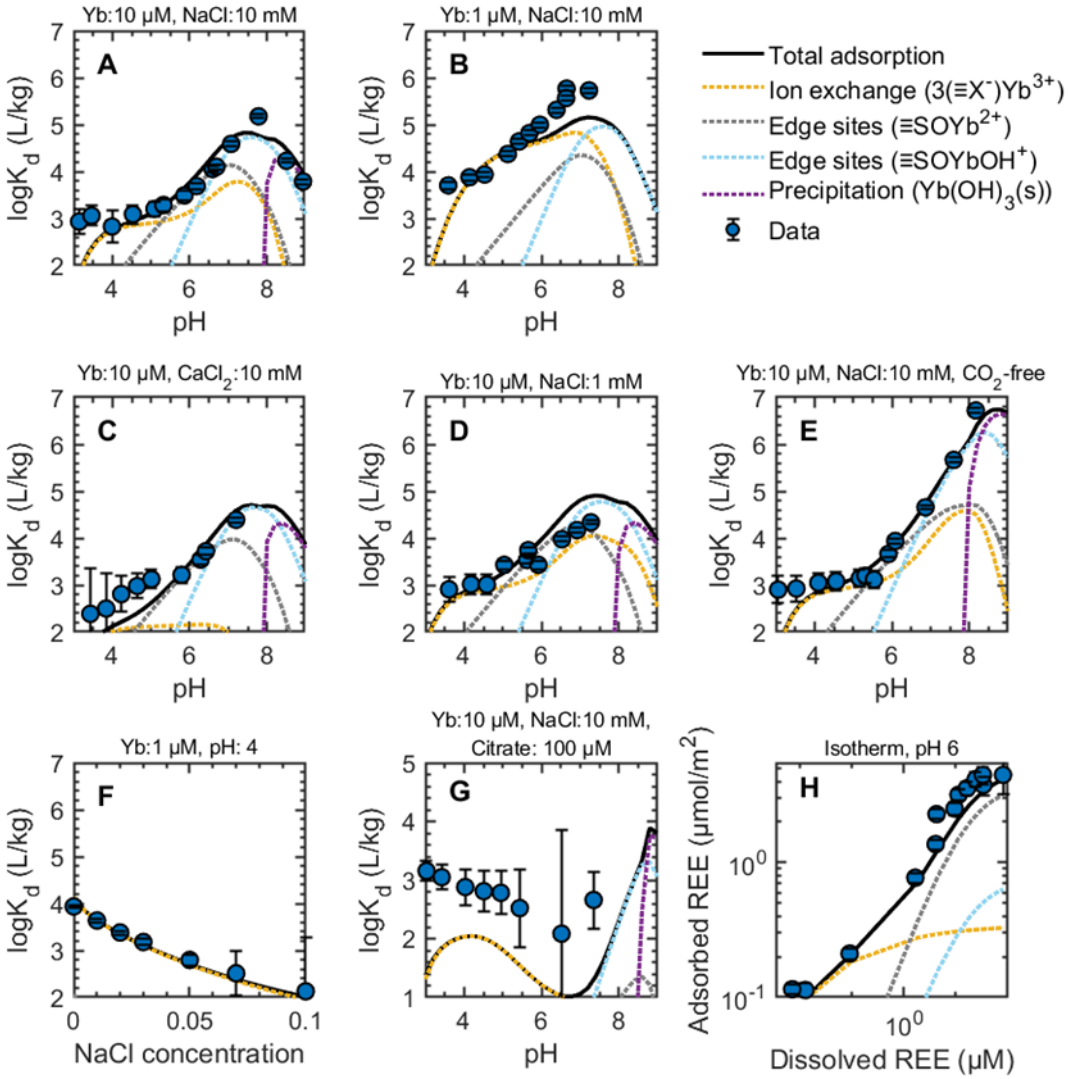

Figure S27. Detailed overview of the NEM-based surface complexation model output (lines) in all experiments with Yb. Markers represent experimental data; open white markers show data points at which solubility calculations indicate the possibility of REE precipitation. DIC in all experiments was in equilibrium with atmospheric CO_2 (except panel E, which corresponds to the CO_2-free experiment).

References

(1) Chorover, J.; Choi, S.; Amistadi, M. K.; Karthikeyan, K. G.; Crosson, G.; Mueller, K. T. Linking Cesium and Strontium Uptake to Kaolinite Weathering in Simulated Tank Waste Leachate. *Environ Sci Technol* **2003**, *37* (10), 2200–2208. https://doi.org/10.1021/es025980x.

(2) Miller, J. N.; Miller, J. C. *Statistics and Chemometrics for Analytical Chemistry*, 6th ed.; Prentice Hall/Pearson: Harlow, 2010.

(3) Klungness, G. D.; Byrne, R. H. Comparative Hydrolysis Behavior of the Rare Earths and Yttrium: The Influence of Temperature and Ionic Strength. *Polyhedron* **2000**, *19* (1), 99–107. https://doi.org/10.1016/S0277-5387(99)00332-0.

(4) National Institute of Standards and Technology. NIST 46.7 Critically Selected Stability Constants of Metal Complexes: Version 8.0, 2004.

(5) Haas, J. R.; Shock, E. L.; Sassani, D. C. Rare Earth Elements in Hydrothermal Systems: Estimates of Standard Partial Molal Thermodynamic Properties of Aqueous Complexes of the Rare Earth Elements at High Pressures and Temperatures. *Geochimica et Cosmochimica Acta* **1995**, *59* (21), 4329–4350. https://doi.org/10.1016/0016-7037(95)00314-P.

(6) Lee, J. H.; Byrne, R. H. Extinction of Comparative Rare Earth Element ~omple~tio~ Behavior Using Linear Free-Energy Relationships. *Geochimica et Cosmochrmica Acta* **1992**, *56*, 1127–1137.

(7) Luo, Y.-R.; Byrne, R. H. Carbonate Complexation of Yttrium and the Rare Earth Elements in Natural Waters. *Geochimica et Cosmochimica Acta* **2004**, *68* (4), 691–699. https://doi.org/10.1016/S0016-7037(03)00495-2.

(8) Millero, F. J. Stability Constants for the Formation of Rare Earth-Inorganic Complexes as a Function of Ionic Strength. *Geochimica et Cosmochimica Acta* **1992**, *56* (8), 3123–3132. https://doi.org/10.1016/0016-7037(92)90293-R.

(9) Smith, R. M.; Martell, A. E. *Critical Stability Constants*; Springer US: Boston, MA, 1989. https://doi.org/10.1007/978-1-4615-6764-6.

(10) Schijf, J.; Byrne, R. H. Stability Constants for Mono- and Dioxalato-Complexes of Y and the REE, Potentially Important Species in Groundwaters and Surface Freshwaters. *Geochimica et Cosmochimica Acta* **2001**, *65* (7), 1037–1046. https://doi.org/10.1016/S0016-7037(00)00591-3.

(11) Spahiu, K.; Bruno, J. *A Selected Thermodynamic Database for REE to Be Used in HLNW Performance Assessment Exercises*; 1995.

(12) Kelly, S. D.; Hesterberg, D.; Ravel, B. Analysis of Soils and Minerals Using X-Ray Absorption Spectroscopy. In *Methods of Soil Analysis Part 5—Mineralogical Methods*; Soil Science Society of America (SSSA) Book Series; John Wiley & Sons, Ltd, 2008; pp 387–463. https://doi.org/10.2136/sssabookser5.5.c14.

(13) Appelo, C. A. J.; Postma, D. *Geochemistry, Groundwater and Pollution*, 2nd ed., 5th corr. repr.; CRC Press: Boca Raton, 2010.

(14) White, G. N.; Zelazny, L. W. Analysis and Implications of the Edge Structure of Dioctahedral Phyllosilicates. *Clays Clay Miner.* **1988**, *36* (2), 141–146. https://doi.org/10.1346/CCMN.1988.0360207.

(15) Sposito, G. *The Surface Chemistry of Soils*; New York : Oxford University Press ; Oxford [Oxfordshire] : Clarendon Press, 1984.

(16) Brady, P. V.; Cygan, R. T.; Nagy, K. L. Molecular Controls on Kaolinite Surface Charge. *Journal of Colloid and Interface Science* **1996**, *183* (2), 356–364. https://doi.org/10.1006/jcis.1996.0557.

(17) Bickmore, B. R.; Nagy, K. L.; Sandlin, P. E.; Crater, T. S. Quantifying Surface Areas of Clays by Atomic Force Microscopy. *American Mineralogist* **2002**, *87* (5–6), 780–783. https://doi.org/10.2138/am-2002-5-622.

(18) Sanders, R. L.; Washton, N. M.; Mueller, K. T. Measurement of the Reactive Surface Area of Clay Minerals Using Solid-State NMR Studies of a Probe Molecule. *J. Phys. Chem. C* **2010**, *114* (12), 5491–5498. https://doi.org/10.1021/jp906132k.

(19) Ward, D. B. Effect of Al and Organic Acids on the Surface Chemistry of Kaolinite. *Clays and Clay Minerals* **1998**, *46* (4), 453–465. https://doi.org/10.1346/CCMN.1998.0460410.

(20) Huertas, F. J.; Chou, L.; Wollast, R. Mechanism of Kaolinite Dissolution at Room Temperature and Pressure: Part 1. Surface Speciation. *Geochimica et Cosmochimica Acta* **1998**, *62* (3), 417–431. https://doi.org/10.1016/S0016-7037(97)00366-9.

(21) Heidmann, I.; Christl, I.; Leu, C.; Kretzschmar, R. Competitive Sorption of Protons and Metal Cations onto Kaolinite: Experiments and Modeling. *Journal of Colloid and Interface Science* **2005**, *282* (2), 270–282. https://doi.org/10.1016/j.jcis.2004.08.019.

(22) Gu, X.; Evans, L. J. Surface Complexation Modelling of Cd(II), Cu(II), Ni(II), Pb(II) and Zn(II) Adsorption onto Kaolinite. *Geochimica et Cosmochimica Acta* **2008**, *72* (2), 267–276. https://doi.org/10.1016/j.gca.2007.09.032.

(23) Lackovic, K.; Johnson, B. B.; Angove, M. J.; Wells, J. D. Modeling the Adsorption of Citric Acid onto Muloorina Illite and Related Clay Minerals. *Journal of Colloid and Interface Science* **2003**, *267* (1), 49–59. https://doi.org/10.1016/S0021-9797(03)00693-3.

(24) Moldoveanu, G. A.; Papangelakis, V. G. Leaching of Lanthanides from Various Weathered Elution Deposited Ores. *Canadian Metallurgical Quarterly* **2013**, *52* (3), 257–264. https://doi.org/10.1179/1879139513Y.0000000060.

(25) Gammons, C. H.; Wood, S. A. The Aqueous Geochemistry of REE. Part 8: Solubility of Ytterbium Oxalate and the Stability of YbžIII/–Oxalate Complexes in Water at 258C to 808C. **2000**.

(26) Wood, S. A. The Aqueous Geochemistry of the Rare-Earth Elements: Critical Stability Constants for Complexes with Simple Carboxylic Acids at 25°C and 1 Bar and Their Application to Nuclear Waste Management. *Eng. Geol.* **1993**, *34* (3), 229–259. https://doi.org/10.1016/0013-7952(93)90092-Q.